Computers and Electronics in Agriculture 232 (2025) 110045

Contents lists available at ScienceDirect

Computers and Electronics in Agriculture

journal homepage: www.elsevier.com/locate/compag

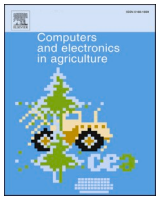

Original papers

A hybrid remotely operated underwater vehicle for maintenance operations in aquaculture: Practical insights from Greek fish farms

Marios Vasileiou [a,b,*], George Vlontzos [b]

[a] Department of Information and Communication Systems Engineering, University of the Aegean, Karlovasi 83200, Samos, Greece
[b] Department of Agriculture, Crop Production and Rural Environment, University of Thessaly, Fytoko, 38446 Volos, Greece

ARTICLE INFO

Keywords:
Marine robotics
Autonomous Underwater Vehicle (AUV)
Remotely Operated Underwater Vehicle (ROV)
Unmanned Underwater Vehicle (UUV)
Digital transformation
Sustainability
Aquaculture

ABSTRACT

Aquaculture serves a pivotal function in catering to the increasing global need for seafood while simultaneously tackling the predicaments posed by the dwindling wild fish reserves. Underwater vehicles have contributed to the expansion of aquaculture by enabling underwater inspections, data collection, and improved maintenance procedures. In addition, underwater vehicles facilitate the acquisition of subsea data, enabling researchers to enhance aquaculture procedures and participate in initiatives aimed at attaining food security. The aim of this work is to design, develop, and evaluate underwater systems for the inspection and maintenance of net cages in aquaculture facilities. The research focuses on developing an underwater vehicle for aquaculture inspection along with the integration of a manipulator to perform maintenance tasks such as removing objects stuck on nets, collecting fish morts, and repairing net tears. This paper provides thorough research on the design of these systems and their applications in aquaculture in Greece. The subsequent focus is directed towards the development of a hybrid remotely operated vehicle, accentuating its software frameworks, modeling, mobility implementation, and navigational capabilities. This system can operate as a tetherless autonomous underwater vehicle for inspection tasks and as a tethered remotely operated vehicle with semi-automatic capabilities for maintenance tasks. In light of this, a tool manipulator is introduced, analyzing its underlying design principles, manipulator capabilities, and electronic integration. The effectiveness and operational capabilities of the underwater vehicle models are substantiated through experimental assessments carried out in Kefalonia fish farms in Greece, resulting in successful missions. The final remarks encapsulate the principal findings obtained from this study, examine their implications, and offer perspectives on forthcoming avenues for subaquatic robotics.

1. Introduction

Aquaculture plays a focal role in meeting the growing worldwide need for seafood while tackling the challenges posed by declining wild fish stocks (FAO, 2020). With the world population continuously growing and the depletion of natural fish populations, aquaculture has emerged as a vital industry for sustainable food production. It offers numerous advantages, including controlled production environments, reduced pressure on wild fish populations, and the potential for localized food production (FAO, 2022). Moreover, aquaculture provides employment opportunities, economic growth, and food security in many regions worldwide. According to a report from the European Commission, aquaculture is experiencing rapid growth, positioning it as the fastest-growing sector within the food production industry (Guillen and Motova, 2013). Furthermore, aquaculture is an essential component of the Blue Transformation strategy of the Food and Agriculture Organization (FAO), which aims to augment the significance of aquatic foods in global food security by implementing eco-friendly policies and practices as well as technological advancements (Blue Food Partnership, 2022). In contrast to its high value and attention, it should be noted that there are some signs that aquaculture will not continue forever, as indicated in Sumaila et al. (2022). This latter is a primary justification for the necessity of enhancing robots utilization in the aquaculture sector moving forward. For aquaculture to fulfill its anticipated significance, current production methods must be enhanced, addressing the industry's diverse issues through clever application of technical tools.

Researchers have traditionally used vessels with instruments, divers, buoys and other platforms to sample the ocean environment using sensors (e.g., current, temperature) or manual sampling (DeVries et al., 2020; Wang et al., 2021). Over the past few years, the range of available

* Corresponding author.
E-mail addresses: mariosvasileiou@uth.gr (M. Vasileiou), gvlontzos@uth.gr (G. Vlontzos).

https://doi.org/10.1016/j.compag.2025.110045
Received 19 September 2024; Received in revised form 23 December 2024; Accepted 26 January 2025
Available online 11 February 2025

instruments for unmanned observation has expanded to encompass Remotely Operated Vehicles (ROVs), Autonomous Underwater Vehicles (AUVs), and Hybrid Remotely Operated Vehicles (HROVs).

ROVs are subaquatic vehicles that are connected to a tether, enabling researchers to conduct observations, collect samples, and perform experiments while remotely controlling the vehicle from the surface (Qiao et al., 2017). They have the capability to remain submerged for long durations, levitate over a specific seafloor objective, or conduct a comprehensive survey of a vast region. A tether links the vehicles to a surface workstation, enabling two-way communication by exchanging control signals, sensor data, and images. This way, the operator can remotely control the vehicle in real-time, enabling precise surveys, collections, and detailed experimentation in the deep ocean (Sitler and Wang, 2022). On the other hand, AUVs are unmanned robotic vehicles that possess the ability to function independently of human intervention. These vehicles are adept at traversing the water utilizing a range of techniques, including drifting, driving, or gliding, contingent upon their unique structural design (Wu et al., 2022). AUVs possess the ability to autonomously alter their mission profile by utilizing environmental data obtained through sensors during their operation.

Subsequently, HROVs have twofold capabilities and can amalgamate the advantageous features of two distinct vehicle types into a unified platform. They can function both as AUVs, navigating without human intervention underwater (Rymansaib et al., 2023), and as ROVs while tethered to a surface station, enabling the remote control of the vehicle by the operator who is located on the surface. This facilitates accurate surveys and samplings, as well as the implementation of intricate experiments in the ocean (Yu et al., 2023).

Over the past decade, there has been a growing interest among researchers in developing robotic systems primarily designed to enhance various aspects of aquaculture processes. Specifically, areas such as quality monitoring and feeding (Von Borstel Luna et al., 2017; Simbeye and Yang, 2014), scrutiny and data acquisition for recirculating aquaculture (Al-Hussaini et al., 2018), fish surveillance (Sung et al., 2014; Chicchon et al., 2023), biomass measurement of fish (Santos-Ballardo et al., 2015), biofouling prevention (Ohrem et al., September 2020), fish farm net cleaning (Bi et al., 2020), and inspection of nets and fish (Amundsen et al., 2021; Lin et al., 2020; Osen et al., 2017), have been identified as potential areas for improvement. Using underwater vehicles for such tasks results in reduced costs associated with human divers while mitigating associated risks. It is important for these robotic systems to prioritize environmentally friendly practices while exhibiting high levels of maneuverability and stability.

In this study, an Unmanned Underwater Vehicle (UUV) for aquaculture inspection called “Kalypso” and a subaquatic manipulator that can be seamlessly integrated with the vehicle to perform tasks such as removing objects from the nets, collecting fish morts, and repairing net tears are presented (Fig. 1). The proposed HROV has twofold capabilities: *(i)* It can function as an AUV featuring autonomous navigation capabilities for aquaculture inspections; and *(ii)* it serves as an ROV for maintenance tasks with assisted operations and semi-automatic capabilities.

The subsequent sections provide an overview of related underwater vehicles for subaquatic operations, the proposed vehicle’s design and manufacturing process, and the implementation of its mobility capabilities, including its modeling. In conclusion, the system is tested as a tool for monitoring current conditions at a commercial fish farm in conjunction with the analysis of flow simulation.

2. Literature review

The continuous technological progress witnessed in the past decade has led to significant advancements in electronics, making them more advanced and affordable. This has provided researchers with the necessary tools to develop innovative designs for underwater vehicles. These vehicles serve various purposes, with the common objective of enhancing underwater operations while minimizing risks to human lives. Some subsea vehicles are designed for heavy-duty tasks (García-Valdovinos et al., 2014; Li et al., 2014), while others specialize in inspecting subaquatic environments (Gotts et al., 2022; Zhao et al., 2022; Ferreira et al., 2018), collecting data on both the surroundings and fish populations (Sung et al., 2014; Santos-Ballardo et al., 2015; Ohrem et al., September 2020). Additionally, there are vehicles that operate in swarms, collaborating to perform specific tasks and exchange information, as well as vehicles that work in tandem with humans underwater. Furthermore, there are vehicles that mimic the movements of

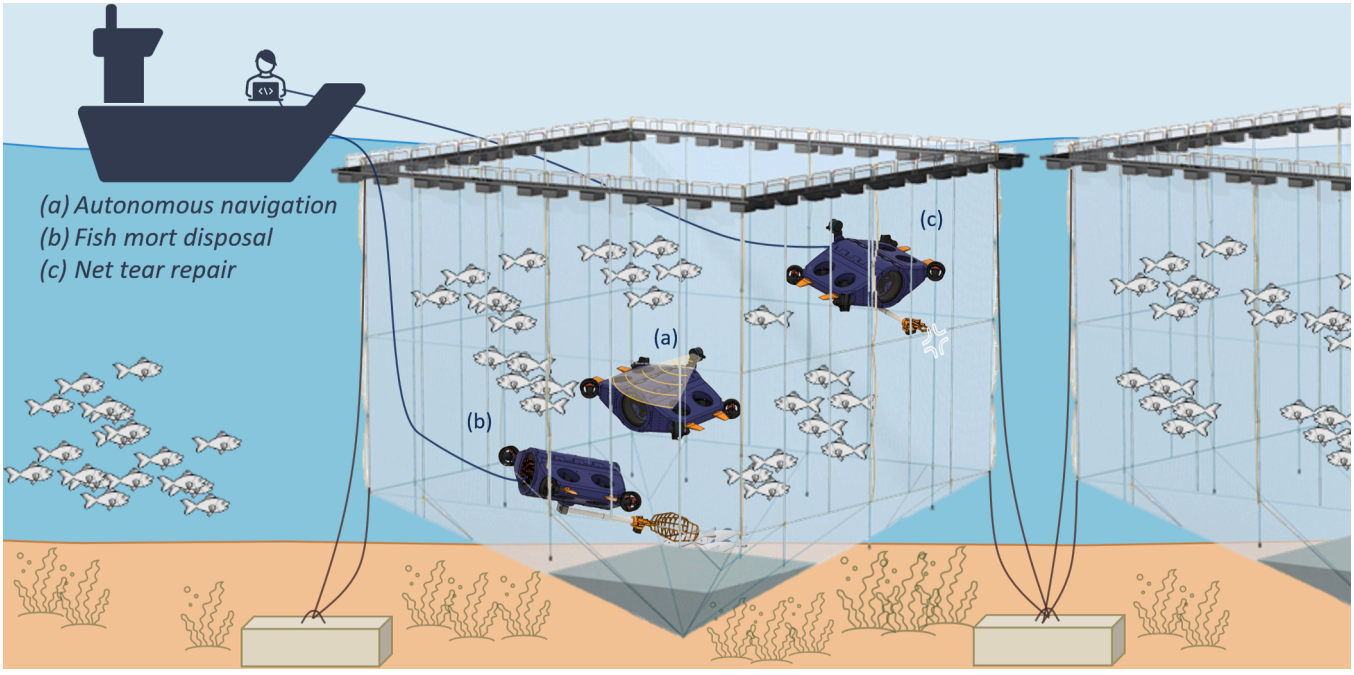

Fig. 1. Overview of the HROV system: (a) tetherless vehicle in autonomous mode; (b) tethered vehicle with fish mort collection tool; (c) tethered vehicle with net repair tool.

fish (Liu and Design, 2020; Arastehfar et al., 2019; Zheng et al., 2013), employing thrusters instead of fins. These underwater vehicles employ sensors that can acquire data on orientation, speed, and depth, enabling efficient and effective operation.

Moreover, marine vehicles are used in complex tasks and utilize various tools or manipulators to carry out more sophisticated underwater tasks. A study conducted by García-Valdovinos et al. (2014) featured an experimental setup involving an ROV that was outfitted with a manipulator to perform heavy-duty tasks. The vehicle features a mechanical passive arm, showcasing a non-linear hydrodynamic model that encompasses relevant parameters and the architecture of its components. Correspondingly, Sitler and Wang (2022) present the development of a versatile and adaptable cable-driven continuum arm that is specifically designed for performing manipulation operations in a free-floating subsea environment. Its mechanical design comprises three key components: a continuum arm, an actuation unit, and a watertight enclosure. Another study introduced a small-sized modular underwater robotic arm that is controlled using a Master-Slave methodology and can be implemented in small-sized ROVs (Barbieri et al., 2018). An alternative approach that suggests employing a compact, deployable, and exceptionally agile ROV as an end effector is introduced in Yu et al. (2013). The primary vehicle would attach this agent ROV through a flexible and intelligent cable that monitors the agent's relative position, eliminating the need for supplementary positioning sensors and enabling a substantial decrease in the agent's overall size.

Furthermore, underwater vehicles face significant challenges in motion control, especially when exposed to unpredictable ocean currents, uncertain parameters, delays in hydraulic systems, and limitations in thrust capabilities. In light of this, a recent study employs an ROV to perform surface cleaning on offshore structures, taking into consideration the challenges of the ocean (Tang et al., 2023). A similar study introduces nonlinear and multivariable control techniques for addressing the trajectory tracking issue of an HROV used for inspection of underwater structures through the measurement of plate thickness (Ferreira et al., 2018). These control strategies are founded on the backstepping methodology and the utilization of the Control Lyapunov Function (CLF). Another aquatic system is modeled to perform operational inspection missions targeting both static and moving objects (Zhao et al., 2022). That research outlines distinct mission profiles that encompass pipeline inspection, inspection of mooring lines for Floating Offshore Wind Turbines (FOWTs) and scanning of circumferential weld surfaces on FOWT spars. In addition, an Autonomous Riser Inspection System (ARIS) as a means to enhance the routine inspection of riser cables, aiming to detect faults at an early stage and collect engineering data to enhance future cable design, is introduced (Gotts et al., 2022). In brief, offshore applications typically experience a more favorable operational environment due to their distance from the coast, resulting in reduced variations in currents and potentially lower current magnitudes, as they are less influenced by tidal currents, and their operation at significant depths, which allows them to evade the wave zone entirely.

Conversely, in aquaculture, operations generally occur in both the wave zone and coastal areas, resulting in significantly greater challenges from waves and currents than in offshore environments. The intricacy of robotic operations in aquaculture is further compounded by the presence of fish, which may experience stress from robots or, in extreme cases, be impacted by them, as well as by the flexible nets and other structural components that deform in response to waves and currents. This results in a significantly more complex environment for autonomous operations compared to the subsea offshore environment. A singular Omnidirectional Surface Vehicle (OSV) is being employed for the purpose of inspecting fish cages by Lin et al. (2020). It has four thrusters and a set of sensors to navigate its surroundings and gather relevant data, while an advanced positioning planning system was devised as an extension of prior research efforts aimed at enhancing aquaculture inspection procedures. In a similar vein, an AUV was designed for conducting inspections in aquaculture by Amundsen et al. (2021). It incorporates a positioning planning system that utilizes Doppler velocity log technology to accurately assess the geometric characteristics of the robot's operational environment. Another ROV that incorporates omnidirectional movement capability through the utilization of three thrusters is presented by Osen et al. (2017). Additionally, a surface vehicle is also introduced as part of this system. By employing a winch situated on the platform, the ROV can be both submerged and subsequently retrieved from the water.

Despite the notable advancements in subaquatic vehicles presented in the literature, critical gaps persist regarding the employment of marine robots in aquaculture. The first gap revolves around the modularity and adaptability of underwater vehicles. While most vehicles boasting increased modularity and adaptability are tailored for swarm applications, emphasizing scalability, those deployed in aquaculture settings predominantly prioritize steadiness, sidelining the crucial aspects of modularity and adaptability (Hackbarth et al., 2015; Duecker et al., 2020; Meyer et al., 2017; Osterloh et al., 2012). This limits the versatility of these vehicles, constraining their capacity to address a diverse array of tasks essential for efficient aquaculture maintenance. A second lacuna emerges in the consideration of energy efficiency and stability in underwater vehicle design. Vehicles intended for swarm applications meticulously address energy efficiency to ensure prolonged operation (Amory and Maehle, 2016; Berlinger et al., 2018; Berlinger et al., 2018; Ridolfi et al., 2016). However, the literature reveals an absence of emphasis on hydrodynamic design in vehicles used within aquaculture. This deficiency impedes the optimization of stability and energy efficiency, undermining the overall effectiveness of these vehicles in navigating and operating efficiently within the dynamic and challenging environments of aquaculture facilities. Furthermore, the literature review exposes a gap in the diversity of underwater manipulator tools. Existing designs are often geared towards specific tasks, leaving a considerable void in the development of manipulators capable of handling a broader range of tools and tasks essential for aquaculture maintenance. Exploring and innovating manipulator designs to accommodate tasks such as fish mort collection and underwater repairs could bridge this gap, enhancing the adaptability and practicality of underwater robotics in the context of aquaculture. Another issue revolves around the coexistence of robots and fish and the impacts of the former to the latter. This has been demonstrated by researchers in both laboratory and commercial farms, elucidating that fish react to the presence and movement of vehicles introduced into the experimental tank or cage (Kruusmaa et al., 2020; Marras and Porfiri, 2012). More specifically, Kruusmaa et al. (2020) investigated salmon behavior in response to different underwater observers, both robots and divers, in a Norwegian aquaculture facility and found that the flipper-propelled robot elicited distinct behavioral responses compared to the thruster-driven one and a human diver, with salmon exhibiting closer proximity at lower tailbeat frequencies; however, variables such as motor noise, color change (yellow to silver), and motion type (active vs. passive) did not significantly affect salmon behavior, highlighting the potential of tailored underwater robots to enhance fish monitoring practices.

Last but not least, a critical aspect is the dearth of real-world implementation. While the literature extensively covers various vehicle designs, the limited exploration of issues faced during actual aquaculture inspections or environmental data collection hampers the translation of theoretical advancements into practical solutions. More specifically, most of the literature presented has applications in experimental sites, such as tanks, pools, etc. This gap underscores the need for more comprehensive studies that provide nuanced perspectives on the challenges encountered in real-world deployments, offering valuable lessons for future researchers and practitioners seeking to refine and optimize underwater robotics for practical use within the intricate and dynamic landscape of aquaculture operations.

In light of these identified gaps, this paper introduces an HROV with capabilities tailored for maintaining aquaculture infrastructures. The main contribution of this study lies in the novel application of an

underwater system in aquaculture, as exemplified in the Kefalonia fish farms in Greece, extending the scope of its usage beyond traditional marine exploration and research to address the specific needs of aquaculture operations. This concept extends the current aquaculture practices, both autonomous inspection tasks (e.g. Amundsen et al., 2021; Osen et al., 2018; Vasileiou et al., 2024), and manipulation tasks (e.g. Brandt et al., 2023; Vasileiou et al., 2023), showcasing the adaptability of an underwater vehicle to navigate, inspect, and maintain net cages. The paper further contributes by presenting a comprehensive design and development process for customized underwater vehicles tailored to the distinctive demands of aquaculture environments. This contribution is particularly significant in bridging the technological divide between general-purpose underwater vehicles and the specialized needs of aquaculture maintenance. Furthermore, an innovative solution introduced in the paper is the concept and design of an underwater arm dedicated to aquaculture maintenance. This underwater arm addresses intricate tasks such as net tear repairs and fish mort disposal, making a substantial contribution to the aquaculture sector. Moreover, the inclusion of modeling, flow simulations, and real-world trials at aquaculture facilities provides empirical evidence of the effectiveness and viability of the developed technologies.

The remainder of this paper is organized as follows. Section 3 presents the design of the vehicle and the tool manipulator. Section 4 quotes the vehicles' modeling, while in section 5 the results are analyzed. Section 6 discusses the proposed system and the application in aquaculture and Section 7 concludes the paper.

3. System design

This section focuses on the design of an underwater vehicle specifically developed for maintenance operations in net cages at aquaculture. The suggested design exhibits adaptability while maintaining cost-effectiveness, rendering it suitable for both manual and automatic operations. The autonomous operations are concentrated on the inspection of the nets, while the manual ones focus on maintenance tasks by utilizing a tool manipulator, such as the extraction of objects entangled in the nets, the disposal of deceased fish, and the repair of any tears (holes) present in the nets. In this section, the design architecture of the vehicle and the tool attachment are described along with their respective components.

3.1. Design architecture

The vehicle is designed to conduct inspection operations of net cages in aquaculture while also adapting seamlessly to satisfy the specific needs of each task. Rapid prototyping and modular assembly facilitates this requiremen through the utilization of 3D printing. Polylactic Acid (PLA) filament is used in 3D printing to produce the exterior body and internal electronic mounts and achive cost-effective and prompt modifications and substitutions. Adaptability is a crucial aspect in fish farming due to the diverse range of operations involved. The vehicle underwent testing in various net cages that exhibited variations in mesh aperture, dimensions, and morphology, including cubic and conical configurations. The present design is developed with the aim of enabling horizontal-lateral movement while impeding vertical oscillation, thereby enhancing its ability to maintain its depth during operation. This movement is the predominant movement performed by the vehicle while inspecting the net cages (left or right motion). To achieve this, the vehicle utilizes distinctive design features, including a flattened top and bottom as well as sloped side sections, to facilitate lateral motion and stability. More specifically, it is designed with a small, inclined surface during lateral movement, resulting in reduced resistance and consequently increased performance (Fig. 2 (a)). At the same time, the effective preservation of its depth is achieved due to the design of the vehicle, as it has a large surface, which increases the resistance during surfacing and diving (Fig. 2 (b)). In light of this, a Computational Fluid Dynamics (CFD) simulation is performed and analyzed in Section 5, while a representation of this notion is given in Fig. 2. This flow modelling was performed during the design of the vehicle, extended to the testing and re-design phase. It was a continuous task in order to optimize the hydrodynamics of the vehicle.

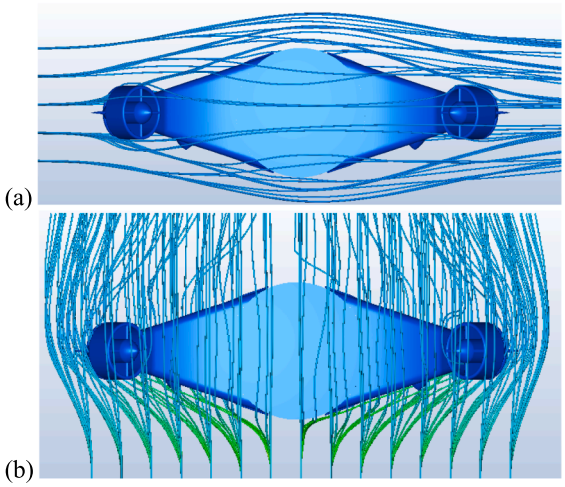

Fig. 2. Fluid flow representation on HROV: *(a)* Lateral motion, *(b)* submerge motion.

Kalypso, weighing approximately twelve kilograms, measures 480x570x182 mm. Its frame comprises three main components. The first component is a watertight enclosure, which houses the electronics that are exposed to water. This enclosure consists of an acrylic tube with a 152 mm inner diameter and 300 mm length, two flanges with three O-rings each, two end caps (one with holes for the cables), and aluminum plugs with O-rings for the cables. The second component comprises side 3D-printed parts that house the vehicle's thrusters and increase the surface area of the robot and thereby its stability. To further stabilize the robot, additional weights (150 g) were inserted into these components, and plastic corks were used to support the top front and rear sections (Fig. 3 parts P1, P2). These side parts thus function as fixed ballast tanks, reducing buoyancy. Moreover, the watertight enclosure and side parts are connected through a 3D-printed mount (Fig. 3 part P3). The vehicle's relatively simple parameterization allows the end user to add or remove components without requiring specialized expertise. Specifically, the vehicle is structured into separate sections, as aforementioned, to simplify the process of maintenance and scalability with supplementary components, such as fins, external sensors, and so on. The parts discussed are also visualized in Fig. A1 in Appendix A.

Furthermore, the HROV has eight motors, four of which are used for vertical motion (M5-M8) and four for horizontal movements (M1-M4), that together provide the vehicle with six (surge, heave, sway, roll pitch, yaw) Degrees of Freedom (DoF) (Fig. 3). In addition, four rotate in a clockwise direction (M3, M4, M6, M7) and the remaining four rotating in an anti-clockwise direction (M1, M2, M5, M8). The design of the vehicle is robust and customizable, and to enhance the stability of the horizontal axis and impede pitch motion, four fins were affixed adjacent to the horizontal motors, as depicted in Fig. 3 (a). Kalypso possesses a symmetrical design that renders it stable in both pitch and roll angles and has slightly positive buoyancy, thereby enabling it to submerge and resurface effortlessly.

In addition, a tool attachment can be affixed to the vehicle in order to enable manipulation tasks underwater. To integrate the tool manipulator, a mounting component is designed to securely attach it to the vehicle, while corks are utilized in order to attain a state of slightly positive buoyancy. The design of the tool manipulator is focused on cost-effectiveness and modularity. It is comprised of components that are easy to replace and produced using 3D-printing and PLA filament. The

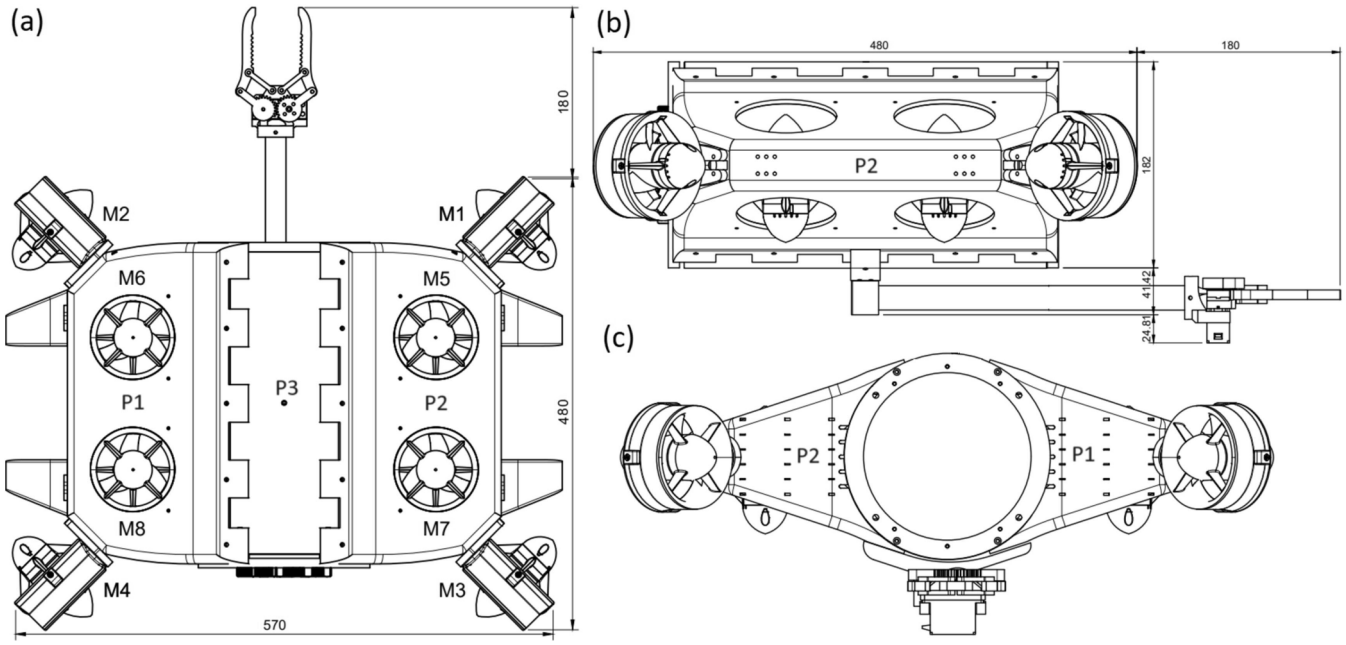

Fig. 3. Conceptual design and dimensions of the vehicle with the tool attachment: *(a)* top view, *(b)* side view, and *(c)* front view (sizes in mm).

purpose of this manipulator is to address three main objectives in aquaculture: *(i)* the extraction of objects entangled in the nets; *(ii)* the collection of deceased fish; and *(iii)* the repair of any tears (holes) present in the nets (Fig. 4). Each use case requires a distinct attachment manipulator. The process involves the interchange of three tool manipulators, which are securely attached to the vehicle using four bolts and nuts. This allows for efficient and robust replacements to be made during operation.

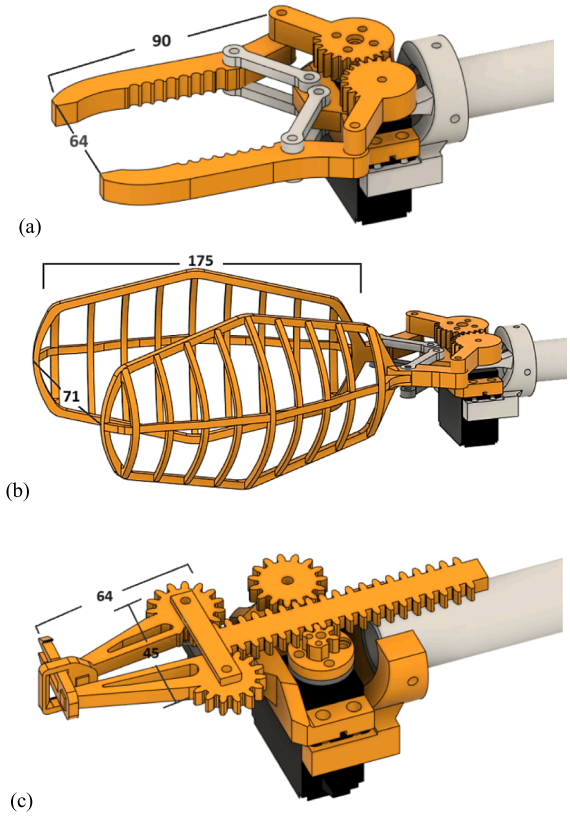

Fig. 4. Tool manipulator attachments: *(a)* Object gripper tool, *(b)* Fish mort grabber tool, *(c)* Net tear repairing tool (sizes in mm).

The first operation involves the utilization of a gripper attachment tool designed for the purpose of removing objects stuck in the nets (Fig. 4 (a)), such as branches and miscellaneous detritus, which possess the potential to induce ruptures in the net or impede the passage of water within the enclosure. The disposal of solid objects, such as branches, can lead to a decrease in net wear, whereas the removal of soft objects, such as seaweed, can enhance water flow within net enclosures, thereby increasing the oxygen levels within the net cages (Stien et al., 2012; Johansson et al., 2007). This tool employs one servo motor with plastic gears to operate the calipers, utilizing the vehicle's DoF to navigate the environment. Therefore, it operates with 6 DoF.

The second operation is about the use of a grabber attachment tool that is capable of retrieving fish morts (Fig. 4 (b)). Fish mortality is a commonly observed phenomenon in aquaculture, which can result in the decomposition of dead fish and subsequent water contamination. Hence, it is crucial to promptly eliminate deceased fish from the surrounding ecosystem in order to mitigate additional pollution. The grabber manipulator facilitates the simple retrieval of morts, which may accumulate on either the surface or the bottom of the net cage. Frequent removal of such debris has the potential to enhance water quality and reduce the probability of fish vandalism (Shakouri, 2003). Similarly with the gripper attachment it utilizes one servo motor and the vehicle's mobility to operate underwater.

The third operation pertains to the utilization of a manipulator attachment tool capable of repairing net tears in aquaculture (Fig. 4 (c)). Net tears can result in fish escapes and product loss, and may serve as vectors for diseases and parasites, intermingling with wild populations and resulting in genetic pollution (Rigby et al., 2017). In order to repair the torn holes, the tool is inserted into the openings of the nets and employs the two calipers to establish connections between the points that have been damaged in the nets. Subsequently, the two calipers become interlocked through the activation of a locking mechanism, rendering them unable to disengage until human intervention is employed for a lasting resolution. Following that, due to its operational mechanism, it becomes detached from its mounting base and persists within the nets, consequently leading to their interconnection. The price of the replacement attachment is approximately €0.40 and is 3D printed with PLA material. The mobility of this tools is also relied on the vehicle

locomotion.

Furthermore, the tool manipulator is intended to function while connected to the vehicle, benefiting from the vehicle's DoF. The specifications of the vehicle and manipulator are quoted in Table 1.

3.2. Appurtenances and software

The vehicle's electronic components can be classified into three distinct groups: (i) submersible components, which can operate underwater; (ii) water-sensitive components, which necessitate protection within a watertight enclosure; and (iii) components located on the surface workstation. The submersible components include thrusters, a pressure sensor, a temperature sensor, lights, and echosounders, while the components housed in watertight enclosures include a mini-PC, Pixhawk PX4 and Raspberry Pi 3 microcontrollers, BLHeli_S 30A Electronic Speed Controllers (ESCs), 14.8 V LiPo batteries, two cameras, a Power Distribution Board (PDB), relays, and leak sensors. In addition, the tool manipulator utilizes a single servo motor that generates the required torque for its operation. The interchange between the operations that require physical interventions (eg. Attachment/removal of the manipulator) is achieved through modular plastic parts and plugs. The vehicle is equipped with suitable plugs that facilitate the interchange of various wires without the need to access the watertight enclosure. This can provide the on-site integration of sensors or the underwater tool manipulator. Each component of the system's software is associated with a dedicated processor board, partitioning it into four primary parts:

- *Pixhawk:* This board is responsible for the control and management of the electronic components integrated within the underwater vehicle, including motors, sensors, and relays. Additionally, it controls the stability of the robot by converting input commands into output signals for the ESCs. The Pixhawk flight controller is integrated with the Ardusub firmware, an open-source software specifically designed for underwater vehicles, and it is configured to support the vehicle with an 8-motor configuration.
- *Mini-PC*: The primary utilization of this computer is for the tetherless autonomous capabilities of the vehicle. More specifically, it is responsible for decision-making and video capture. The connection between the mini-PC and the Pixhawk is established through a USB port, with communication facilitated by the utilization of the Mavlink protocol. Also, it has Ubuntu software installed, and Python 3 scripts are used to communicate with the Pixhawk.
- *Topside PC*: This PC serves as a means of remote control for the robot, allowing operators to manipulate its movements from a distance. Additionally, the interface software on this computer facilitates the display of streamed video, providing a visual representation of the vehicle's surroundings. Moreover, it can serve as an alternative for the mini-PC when tethered and is equipped with QGroundControl, an interface that facilitates seamless communication with the robot during remote control operations. The vehicle has the capability to designate a single computer as its primary control unit depending on whether it is operating in a tethered or tetherless mode, and the inclusion of a server becomes imperative as an intermediary component to establish a connection with the Pixhawk.
- *Raspberry Pi*: It functions as a server and facilitates data exchange between the topside computer/mini-PC and the Pixhawk through an Ethernet connection. When tethered, it utilizes the Mavlink protocol for communication with the Pixhawk and the UDP protocol to transmit video feedback to the topside computer.

Table 1
Specifications of the HROV.

Specification	HROV w/o manipulator	HROV with tool manipulator		
		Gripper tool	Grabber tool	Repairing tool
Application	Inspection	Object removal	Fish mort disposal	Net tear repair
Dimensions ($L \times W \times H$)	480 × 570 × 182 mm	660 × 570 × 248 mm	765 × 570 × 248 mm	650 × 570 × 248 mm
Weight	12.3 kg	12.7 kg (390 g)	12.7 kg (410 g)	12.6 kg (325 g)
Battery capacity	20 Ah	20 Ah	20 Ah	20 Ah
DoF	6	6	6	6
Number of motors	8	9 (8 + 1)	9 (8 + 1)	9 (8 + 1)
Rotational speed (roll–pitch–yaw)	135 – 125 – 330 deg/s	N/A	N/A	N/A
Translational speed (surge–heave–sway)	1.2 – 0.5 – 1.4 m/s	N/A	N/A	N/A
Total cost	4050 €	4075 €	4080 €	4075 €

The HROV can navigate through its environment using either manual control or autonomous operation. In autonomous operation, the vehicle has the capability to operate either with or without a tether, as the control is managed by the Mini-PC. On the other hand, in manual operation, it is necessary for the vehicle to be tethered in order to establish communication. Fig. 5 displays a simplified data flow diagram to illustrate the processes conducted among the processors. The processes at the surface workstation are executed when the vehicle is tethered and controlled by the user. When the vehicle operates in tetherless autonomous mode, the surface workstation is not required.

4. Modeling

This section focuses on the dynamic models pertaining to Kalypso. This paper employs fundamental theories to model Kalypso in a similar rationale as expounded in detail in Fossen's Handbook (Fossen, 2011), which provides mathematical models for various types of marine vessels. The field of dynamics can be bifurcated into two distinct domains: kinematics, which exclusively deals with the geometric facets of motion, and kinetics, which involves the examination of the forces that instigate the motion.

4.1. Kinematics modeling

4.1.1. Reference frames

In the analysis of Kalypso's motion with six DoF, it is advantageous to determine two reference frames. Specifically:

- *North-East-Down* (NED) coordinate system: It has origin O_N and axes $\{n\} = (x_n, y_n, z_n)$. This system denotes the physical environment where the axes x_n, y_n, and Z_n align with the north, east, and downward directions perpendicular to the Earth's surface, correspondingly. The point of origin O_N is established at a position of arbitrary latitude and longitude. In the case of Kalypso, which operates within a limited geographical region characterized by relatively constant longitude and latitude, navigation is facilitated through the utilization of an earth-fixed tangent plane situated on the surface. The navigational technique commonly known as flat earth navigation (Fossen, 2011) shall henceforth be designated as $\{n\}$. In light of this, it is possible to make the assumption that $\{n\}$ remains inertial, thereby allowing for the continued application of Newton's laws. Therefore, an inertial reference frame is used with the origin O_I and axes $\{n\} = (x_n, y_n, z_n)$.
- Body-fixed reference frame: It has an origin O_B and axes $\{b\} = (x_b, y_b, z_b)$. This reference frame is a mobile coordinate system that remains stationary relative to the vehicle. The geometric center of the vehicle is designated as the origin O_B to take advantage of inherent physical symmetries. The vehicle's spatial pose is denoted in relation to the inertial reference frame O_I, whereas its linear and angular velocities must be articulated in the coordinate system fixed to the body.

The transformation of a vector from one coordinate frame to another

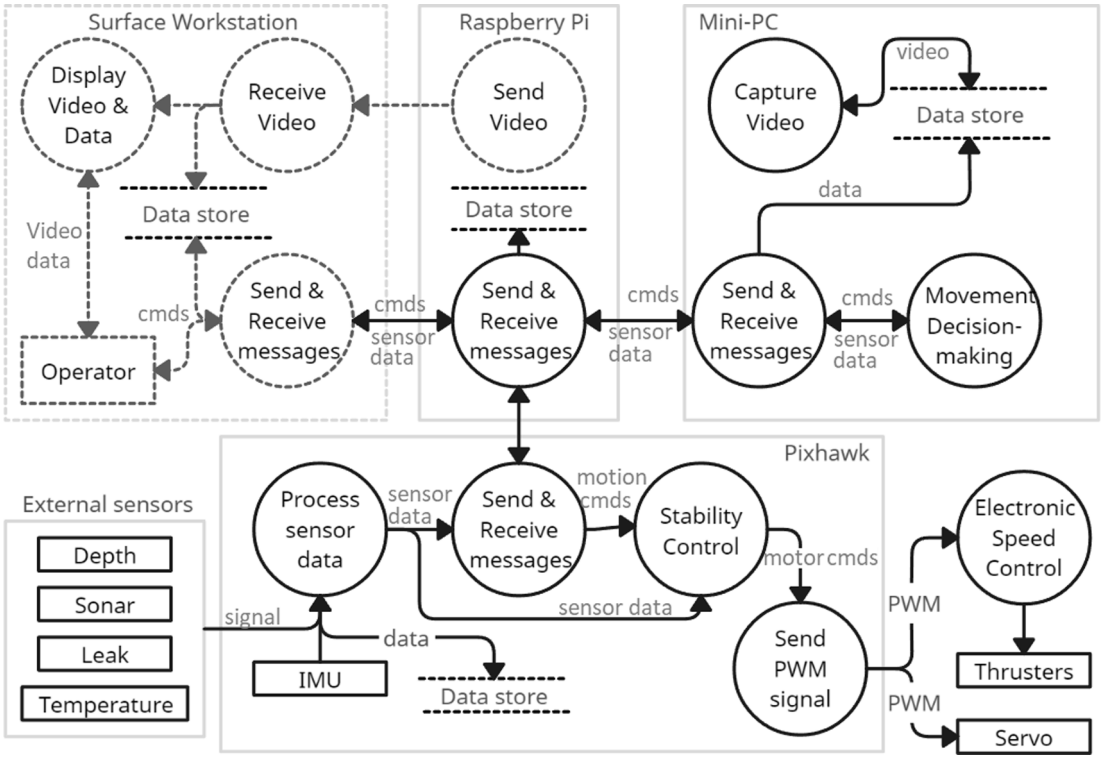

Fig. 5. Simplified Data Flow Diagram of the proposed system.

can be achieved through the application of a rotation matrix. An example of vector transformation can be demonstrated by considering a vector V in reference frame x, denoted as $V^x \in \mathbb{R}^3$. By utilizing the rotation matrix R_x^y, the vector V can be transformed to the reference frame y, represented as $V^y \in \mathbb{R}^3$. The operation of transforming a vector V from one reference frame x to another reference frame y is expressed by Eq. (1) as stated in (Wu, 2018).

$$V^y = R_x^y V^x \tag{1}$$

4.1.2. Motions and notations

The vectorial representation of Kalypso's motion in six degrees of freedom can be achieved through the use of notation denoted by the Society of Naval Architects and Marine Engineers (SNAME), as outlined in the literature (Wu, 2018; Fossen, 2011; SNAME, 1950). This notation employs six coordinates to determine the vehicle's position and orientation, with their respective time derivatives serving to describe the linear and angular velocities of the ROV.

The eight-thruster configuration of Kalypso enables it to achieve six DoF, including the ability to perform surge, heave, and sway translational motions, as well as roll, pitch, and yaw rotational motions (Fig. 6). "Surge" refers to the linear longitudinal displacement, which is generated by four horizontally positioned thrusters at a 45-degree angle. By employing the same horizontally positioned thrusters, the vehicle can execute "sway" motion, which refers to the linear transverse displacement along the Y axis (lateral). The linear vertical (up/down) movement is achieved by "heave" through the utilization of four thrusters on the vertical plane. In a similar vein, the robot employs its four vertical thrusters to execute a tilting rotation around its longitudinal (X) axis, thus effecting a "roll" movement, and an up/down rotation around its transverse (Y) axis, thereby achieving a "pitch" rotation. "Yaw" movement is achieved through control of the four horizontal motors, resulting in a rotation about its vertical (Z) axis.

Subsequently, the following vectors, Eq. (2), (3), address the velocities and positions respectively:

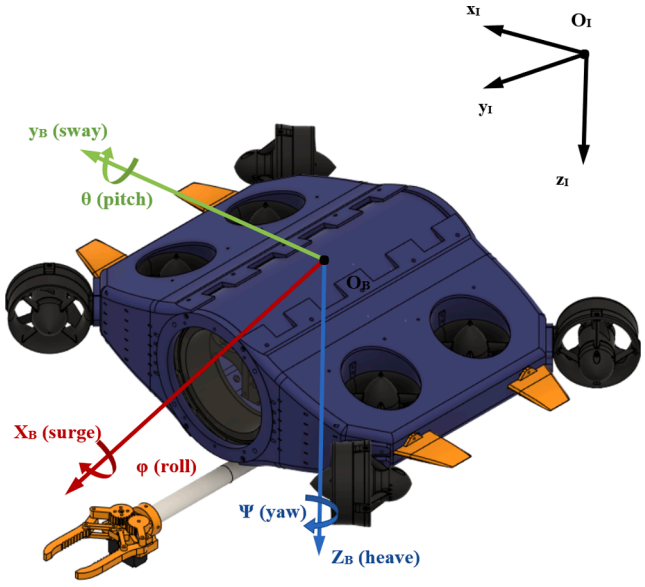

Fig. 6. Coordinate frames and Motions of the vehicle.

$$\nu = [u\, v\, w\, p\, q\, r]^T \in \mathbb{R}^6 \tag{2}$$

$$\eta = [x\, y\, z\, \phi\, \theta\, \psi]^T \in \mathbb{R}^3 \times S^3 \tag{3}$$

where $\mathbb{R}^6$ is the six-dimensional Euclidean space and S^3 denotes the sphere in which the three angles ϕ, ψ, Θ are defined on the interval $S = [0, 2\pi]$. Therefore, the system's order is 12.

Furthermore, the force vector that correlates to the six DoF is expressed by Eq. (4), which characterizes the moments and forces that are exerted on the underwater vehicle.

$$\tau = [X, Y, Z, K, M, N]^T \tag{4}$$

Thus, the overall movement of a Kalypso in six DoF can be delineated by the subsequent vectors:

$$\text{Orientation \& position} : \eta = \begin{bmatrix} p \\ \theta \end{bmatrix} \tag{5}$$

$$\text{Linear \& angular velocity} : \nu = \begin{bmatrix} v \\ \omega \end{bmatrix} \tag{6}$$

$$\text{Moment \& force} : \tau = \begin{bmatrix} f \\ m \end{bmatrix} \tag{7}$$

4.1.3. Reference frames' transformations

In this subsection, the transformations between BODY *{b}* and NED *{n}* are presented with the Euler Angle Transformation. The linear velocities' transformation from BODY to NED is as follows:

$$v^n = R_b^n(\Theta)v^b \tag{8}$$

where v is the linear velocity vector of each frame, while $R_b^n(\Theta)$ denotes the rotation matrix from *{b}* to *{n}* calculated as follows:

$$R_b^n(\Theta) = R_z(\psi)R_y(\theta)R_x(\varphi) \tag{9}$$

Likewise, the conversion of angular velocities is expressed as (Kadiyam et al., 2020):

$$\dot{\Theta} = \mathrm{T}_\Theta(\Theta)\omega^b \tag{10}$$

Eq. (10) pertains to the angular velocity vectors ω and Θ in *{b}* and *{n}* respectively. The angular transformation matrix from *{b}* to *{n}* is denoted as $\mathrm{T}_\Theta(\Theta)$.

$$T_\Theta(\Theta) = \begin{bmatrix} 1 & \sin\varphi\tan\theta & \cos\phi\tan\theta \\ 0 & \cos\varphi & -\sin\varphi \\ 0 & \dfrac{\sin\varphi}{\cos\theta} & \dfrac{\cos\varphi}{\cos\theta} \end{bmatrix} \tag{11}$$

Subsequently, the kinematic equation for 6 DoF can be expressed in a vector format as follows:

$$\dot{\eta} = J_q(\eta)v \Leftrightarrow \begin{bmatrix} \dot{p} \\ \dot{\Theta} \end{bmatrix} = \begin{bmatrix} R_b^n(\Theta) & 0_{3\times3} \\ 0_{3\times3} & \mathrm{T}_\Theta(\Theta) \end{bmatrix} \begin{bmatrix} v^b \\ \omega^b \end{bmatrix} \tag{12}$$

Thus, the conversion matrix that maps the vehicle's body frame to the NED global reference frame through Euler angle transformation can be expressed as follows:

$$J_\Theta(\eta) = \begin{bmatrix} R_b^n(\Theta) & 0_{3\times3} \\ 0_{3\times3} & \mathrm{T}_\Theta(\Theta) \end{bmatrix} \tag{13}$$

4.2. Kinetics modeling

The kinetics of a rigid body is the study of the motion and forces of solid objects without deformation. The derivation of the equations of motion for Kalypso requires a comprehensive examination of the dynamics of rigid bodies, as well as an analysis of hydrodynamics and hydrostatics. The primary objective of this subsection is to demonstrate the principles of Kalypso's kinetics that can be articulated within a vectorial framework in a similar rationale as Fossen (2011).

4.2.1. Motion of the vehicle

Considering the water currents, and that both M and (ν) comprise of components related to rigid-body dynamics and hydrodynamics, the model is conveyed as follows (Wu, 2018):

$$M_{RB}\dot{\nu} + C_{RB}(\nu)\nu + M_A\dot{\nu}_w + C_A(\nu_w)\nu_w + D(\nu_w)\nu_w + g(\eta) = \tau \tag{14}$$

where $M_A, M_{RB} \in \mathbb{R}^{6x6}$ which represent the added mass and rigid-body matrices, respectively. In addition, the matrix $C_{RB}(\nu) \in \mathbb{R}^{6x6}$ represents the Coriolis and centripetal effects caused by the rotation of the body frame around the NED world frame, induced by M_{RB}. Similarly, the matrix $C_A(\nu_w) \in \mathbb{R}^{6x6}$ represents the Coriolis and centripetal effects caused by the rotation of the body frame around the NED world frame, induced by M_A. The relative velocity vector ν_w is used to determine these effects as follows:

$$\nu_w = \nu - \nu_c \tag{15}$$

The computation of the rigid-body mass matrix is conducted in accordance with the derivation of equations of motion for rigid bodies through the application of Newtonian formulation as outlined by Fossen (2011) and Li et al. (2023):

$$M_{RB} = \begin{bmatrix} m & -mS\left(r_g^b\right) \\ mS\left(r_g^b\right) & I_b \end{bmatrix} \tag{16}$$

$$M_{RB} = \begin{bmatrix} m & 0 & 0 & 0 & mz_g & -my_g \\ 0 & m & 0 & -mz_g & 0 & mx_g \\ 0 & 0 & m & my_g & -mx_g & 0 \\ 0 & -mz_g & my_g & I_x & -I_{xy} & -I_{xz} \\ mz_g & 0 & -mx_g & -I_{yx} & I_y & -I_{yz} \\ -my_g & mx_g & 0 & -I_{zx} & -I_{zy} & I_z \end{bmatrix} \tag{17}$$

The Coriolis and centripetal matrix $C_{RB}(\nu)$ for a rigid body is then obtained by performing the skew-symmetric cross-product operation on M_{RB}, as indicated by Wu (2018) and shown below:

$$C_{RB}(\nu) = \begin{bmatrix} 0 & 0 & 0 & 0 & mw & 0 \\ 0 & 0 & 0 & -mw & 0 & 0 \\ 0 & 0 & 0 & mv & -mu & 0 \\ 0 & mw & -mv & 0 & I_z r & -I_y q \\ -mw & 0 & -mu & -I_z r & 0 & -I_x p \\ mv & -mu & 0 & I_y q & -I_x p & 0 \end{bmatrix} \tag{18}$$

4.2.2. Hydrodynamics

The study of the fluid mechanics principles governing the motion of a vehicle through a fluid medium is denoted as hydrodynamics. The added mass matrix M_A, the added mass Coriolis, and centripetal matrix $C_A(\nu)$ can be obtained in hydrodynamic contexts through the utilization of an energy-based approach that relies on Kirchhoff's equation (Fossen, 2011). The determination of the added mass of Kalypso in a fluid is based on the utilization of the added mass matrix M_A with $M_A = M_A^T$ (Wu, 2018), which is expressed as:

$$M_A = -\begin{bmatrix} X_{\dot{u}} & X_{\dot{v}} & X_{\dot{w}} & X_{\dot{p}} & X_{\dot{q}} & X_{\dot{r}} \\ Y_{\dot{u}} & Y_{\dot{v}} & Y_{\dot{w}} & Y_{\dot{p}} & Y_{\dot{q}} & Y_{\dot{r}} \\ Z_{\dot{u}} & Z_{\dot{v}} & Z_{\dot{w}} & Z_{\dot{p}} & Z_{\dot{q}} & Z_{\dot{r}} \\ K_{\dot{u}} & K_{\dot{v}} & K_{\dot{w}} & K_{\dot{p}} & K_{\dot{q}} & K_{\dot{r}} \\ M_{\dot{u}} & M_{\dot{v}} & M_{\dot{w}} & M_{\dot{p}} & M_{\dot{q}} & M_{\dot{r}} \\ N_{\dot{u}} & N_{\dot{v}} & N_{\dot{w}} & N_{\dot{p}} & N_{\dot{q}} & N_{\dot{r}} \end{bmatrix} \tag{19}$$

The notation by SNAME, which was introduced in section 4.1.2 is utilized to represent the hydrodynamic derivatives. The hydrodynamic derivative, denoted as $Z_{\dot{u}}$, pertains to the hydrodynamic added mass force Z in the vertical direction (heave) that results from an acceleration u along the horizontal axis (surge). This can be expressed mathematically as:

$$Z_{\dot{u}} = \frac{\partial Z}{\partial \dot{u}} \tag{20}$$

For the majority of practical scenarios, the off-diagonal elements of the matrix M_A exhibit relatively smaller magnitudes in comparison to the diagonal elements. Specifically, it is assumed that the movements between the DoF of Kalypso in hydrodynamics are decoupled, thereby allowing for the neglect of the off-diagonal terms of the M_A matrix.

Consequently, it is possible to simplify the added mass matrix, denoted as M_A as follows (Hammoud et al., 2021):

$$M_A = -\begin{bmatrix} X_{\dot{u}} & 0 & 0 & 0 & 0 & 0 \\ 0 & Y_{\dot{v}} & 0 & 0 & 0 & 0 \\ 0 & 0 & Z_{\dot{w}} & 0 & 0 & 0 \\ 0 & 0 & 0 & K_{\dot{p}} & 0 & 0 \\ 0 & 0 & 0 & 0 & M_{\dot{q}} & 0 \\ 0 & 0 & 0 & 0 & 0 & N_{\dot{r}} \end{bmatrix} \tag{21}$$

Subsequently, the Eq. (22) for the $C_A(\nu)$ matrix can be derived, which is the nonlinear hydrodynamic Coriolis and centripetal matrix as a function of the additional mass (Kadiyam et al., 2020):

$$C_A(\nu) = -\begin{bmatrix} 0 & 0 & 0 & 0 & z_{\dot{w}}w & 0 \\ 0 & 0 & 0 & -z_{\dot{w}}w & 0 & -X_{\dot{u}}u \\ 0 & 0 & 0 & -Y_{\dot{u}}v & X_{\dot{u}}u & 0 \\ 0 & -z_{\dot{w}}w & Y_{\dot{u}}v & 0 & -N_{\dot{r}}r & M_{\dot{q}}q \\ z_{\dot{w}}w & 0 & -X_{\dot{u}}u & N_{\dot{r}}r & 0 & -K_{\dot{p}}p \\ -Y_{\dot{u}}v & X_{\dot{u}}u & 0 & -M_{\dot{q}}q & K_{\dot{p}}p & 0 \end{bmatrix} \tag{22}$$

Furthermore, a marine vessel's hydrodynamic damping is primarily attributed to one of four primary sources: potential damping, wave drift damping, skin friction, or damping due to vortex shedding (Fossen, 2011). The damping of an underwater vehicle, denoted as $D(\nu)$, can be estimated by a combination of a linear damping D_L, which arises from skin friction, and a quadratic damping term $D_{NL}(\nu)$, primarily caused by vortex shedding. This approximation is expressed as follows:

$$D(\nu) = D_L + D_{NL}(\nu) \tag{23}$$

Correspondingly, the diagonalization of the damping matrix is achieved through decoupling, resulting in the linear and quadratic damping matrices being expressed as Eq. (24) and Eq. (25), respectively (Wu, 2018).

$$D_L = -diag[X_u,\ Y_v,\ Z_w, K_p,\ M_q,\ N_r] \tag{24}$$

$$D_{NL}(\nu) = -diag[X_{u|u|}|u|,\ Y_{v|v|}|v|,\ Z_{w|w|}|w|, K_{p|p|}|p|,\ M_{q|q|}|q|,\ N_{r|r|}|r|] \tag{25}$$

The values of D_L and $D_{NL}(\nu)$ are ascertained through experiments. Therefore, the comprehensive hydrodynamic damping matrix $D(\nu)$ is derived as follows:

$$D(\nu) = -\begin{bmatrix} X_u + X_{u|u|}|u| & 0 & 0 & 0 & 0 & 0 \\ 0 & Y_v + Y_{v|v|}|v| & 0 & 0 & 0 & 0 \\ 0 & 0 & Z_w + Z_{w|w|}|w| & 0 & 0 & 0 \\ 0 & 0 & 0 & K_p + K_{p|p|}|p| & 0 & 0 \\ 0 & 0 & 0 & 0 & M_q + M_{q|q|}|q| & 0 \\ 0 & 0 & 0 & 0 & 0 & N_r + N_{r|r|}|r| \end{bmatrix} \tag{26}$$

4.2.3. Hydrostatics

Hydrostatics is a subfield of physics that pertains to the properties of fluids in a state of rest, with a specific focus on the pressure within a fluid or the pressure exerted by a fluid on an object that is submerged within it (Mansour et al., 2008). In the field of hydrostatics, the restoring forces that act upon a marine vehicle as a result of gravitational and buoyancy forces are referred to as such. The weight of a body W and buoyancy force B are determined in Eq. (27), (28) by utilizing the following variables:

m: represents the mass of the vehicle,

g: represents the acceleration of gravity,

ρ: represents the density of water,

∇: represents the volume of fluid displaced by the vehicle.

$$W = mg \tag{27}$$

$$B = \rho g \nabla \tag{28}$$

The vehicle's center of buoyancy is denoted as follows:

$$r_b = [x_b,\ y_b,\ z_b]^T \tag{29}$$

The physical and geometrical parameters are quoted in Table 2.

The placement of the Kalypso's body frame at the center of buoyancy results in the calculation of r_b as follows:

$$r_b = [0,\ 0,\ 0]^T \tag{30}$$

In addition, due to Kalypso's symmetry in both the xz-plane and xy-plane, the calculation for the position of the center of gravity of Kalypso, denoted as r_g, is expressed in a similar rationale as in Wu (2018) as follows:

$$r_g = [x_g\ y_g\ z_g]^T = [0,\ 0,\ z_g]^T \tag{31}$$

The calculation of the overall restoring force vector $g(\eta)$ can be achieved through the utilization of Euler angle transformation, as expressed in the following equation:

$$g(\eta) = \begin{bmatrix} (W-B)\sin\theta \\ -(W-B)\cos\theta\sin\phi \\ -(W-B)\cos\theta\sin\phi \\ z_g W\cos\theta\sin\phi \\ z_g W\sin\theta \\ 0 \end{bmatrix} \tag{32}$$

4.3. Control allocation

Control allocation is a crucial aspect in the field of control engineering. It refers to the process of distributing control commands among various actuators in a system with the aim of achieving desired control objectives.

As illustrated in Fig. 7, Kalypso is outfitted with a total of eight thrusters that produce varying forces in distinct directions. Thus, Kalypso possesses six DoFs and is equipped with eight control inputs.

The application of forces can be represented mathematically through the use of a vector $F = [F^1,\ldots,\ F^8]^T$, while the control inputs are expressed as $u = [u^1,\ldots,\ u^8]^T$. The thrust coefficient is denoted as $K = diag[K^1,\ldots,\ K^8]$. As stated by Muzammal et al. (2021) the representation of the control force is expressed by $F = Ku$, while the forces and moments are described by Eq. (43) where:

$$\tau = \begin{bmatrix} f \\ r \times f \end{bmatrix} = \begin{bmatrix} F_x \\ F_y \\ F_z \\ F_z l_y - F_y l_z \\ F_x l_z - F_z l_x \\ F_y l_x - F_x l_y \end{bmatrix} \tag{33}$$

Therefore, since Kalypso is equipped with 8 thrusters, the generalized forces and moments in six DoF ($\tau \in \mathbb{R}^6$) resulting from the thrusters can be expressed as a function of the control inputs ($u \in \mathbb{R}^8$). This can be modeled as follows:

$$\tau = T(a)\, F = T(a) K u \tag{34}$$

where the thrust configuration matrix is:

$$T = [t_1, t_2, t_3, t_4, t_5, t_6, t_7, t_8] \in \mathbb{R}^{6\times 8} \tag{35}$$

and the vector representing the angle of thrust rotation is represented as $T(a)$ with $a \in \mathbb{R}^8$.

In addition, the angles at which the horizontal motors (T_1 to T_4) are installed are as follows respectively: 45°, −45°, −135°, and 135°. Fig. 7 depicts the l_{x1} and l_{y1} moments of the thrusters, respectively. It is noteworthy that the l_{z1} moment is zero, as the center of gravity is aligned with the motors' height. Furthermore, F_{z1} is equivalent to zero as the horizontal motors do not exert any influence on the z-axis. The moments and forces of the remaining motors were calculated the same way following Eq. (33) and can be seen in Eq. (36).

$$\tau = \begin{bmatrix} 0.707 & 0.707 & -0.707 & -0.707 & 0 & 0 & 0 & 0 \\ -0.707 & 0.707 & -0.707 & 0.707 & 0 & 0 & 0 & 0 \\ 0 & 0 & 0 & 0 & -1 & 1 & 1 & -1 \\ 0 & 0 & 0 & 0 & -0.160 & -0.160 & 0.160 & 0.160 \\ 0 & 0 & 0 & 0 & 0.0695 & -0.0695 & 0.0695 & -0.0695 \\ -0.3 & 0.3 & 0.3 & -0.3 & 0 & 0 & 0 & 0 \end{bmatrix} \begin{bmatrix} F_1 \\ F_2 \\ F_3 \\ F_4 \\ F_5 \\ F_6 \\ F_7 \\ F_8 \end{bmatrix} \tag{36}$$

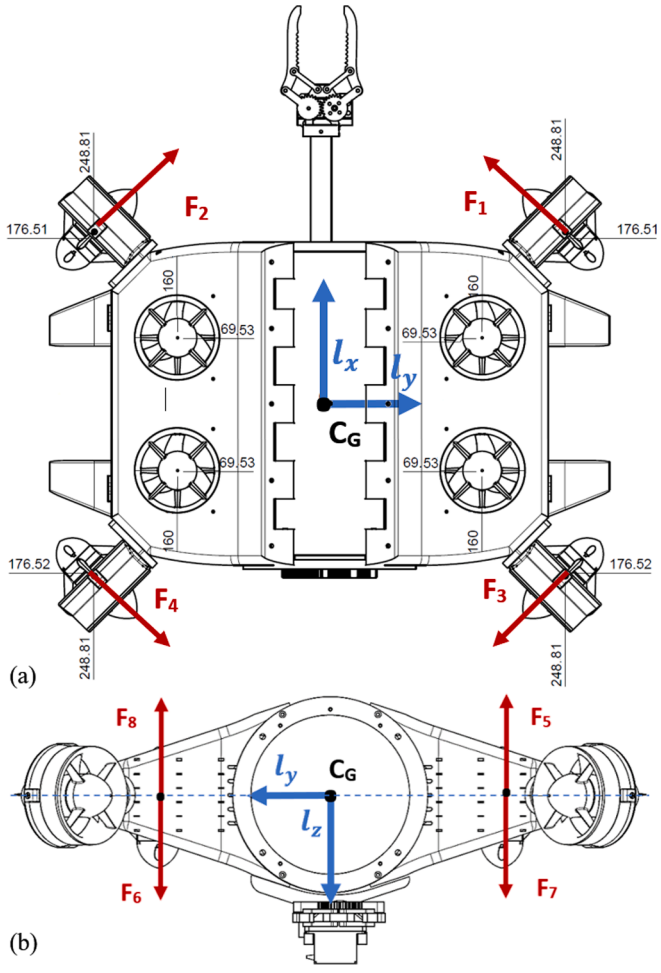

Fig. 7. Forces acting on the vehicle: *(a)* Top view, *(b)* Front view.

The moments of all motors are quoted in Table 3.

In addition, the process of control allocation involves the computation of the control input signal, denoted as u, which is subsequently applied to the thrusters. This is done with the aim of achieving a generalized expression for the overall desired control forces, represented as τ. The control input vector can be obtained by expressing the control forces and moments resulting from thrusters in relation to control inputs, as indicated by Eq. (34), and with the application of Moore-Penrose pseudo-inverse T^+ which is necessary for the non-square thrust configuration matrix T of Kalypso in a similar manner as in (Wu, 2018):

$$u = K^{-1} T^{+1} \tau \tag{37}$$

Moreover, Kalypso undergoes a drag force C_D. The force denoted as F_D is dependent on three factors, namely: *(i)* the velocity v between the AUV and the seawater, *(ii)* the density ρ_{sw} of the seawater, and *(iii)* the projected area A (Sønstabø, 2017) as given by:

$$C_D = \frac{2 \bullet F_D}{v^2 \bullet \rho_{sw} \bullet A} \tag{38}$$

4.4. Locomotion

To conduct inspection tasks within net cages at aquaculture, an underwater vehicle must traverse considerable distances while ensuring consistent stability in its robotic orientation and net entanglement avoidance, irrespective of prevailing ocean currents, while maintaining optimal energy consumption efficiency. In addition to Kalypso's ability to maintain its orientation, it possesses the capability to stabilize itself in any position, encompassing a full 360 degrees around all axes. In this manner, it can perform maintenance tasks on the net cages from various perspectives, such as the bottom of the net cage.

4.4.1. Autonomous navigation and EKF estimations

Furthermore, the vehicle exhibits autonomous navigation within the fish cage by leveraging the distance sensors and the Inertial Measurement Unit (IMU) sensor. The Pixhawk flight controller employs an Extended Kalman filter (EKF) to generate a state estimation, relying on the integrated IMU. The EKF is a recursive algorithm used to estimate

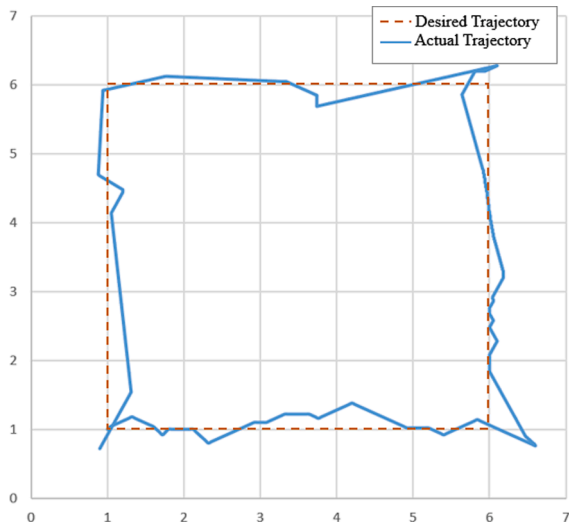

Fig. 8. Visualization of the vehicle trajectory within a square net cage in 2D.

the state of a dynamic system from a series of noisy measurements (Tiwari and Krishnankutty, 2021). It's an extension of the Kalman Filter, designed to handle non-linear systems (Rigatos et al., 2020). The traditional Kalman Filter is highly effective for linear systems, but many real-world systems exhibit non-linear behavior. The EKF addresses this limitation by linearizing the system equations at each iteration and is commonly used for state estimation in non-linear systems, and its equations involve predicting the state of a system and updating this prediction based on noisy measurements. (Rowan, 2023).

The Estimation and Control Library (ECL) employed utilizes an EKF algorithm to process sensor measurements and provide estimations for various states (PX4 Autopilot PX4-ECL GitHub Library, 2024), including the quaternion representing the rotation from the local earth frame (North, East, Down) to the body frame (X, Y, Z) denoted as:

$$q_{NED-B} = [q_0, q_1, q_2, q_3] \tag{39}$$

where q_0 is the scalar part and q_1, q_2, q_3 are the vector part.

The EKF operates with a time delay known as the 'fusion time horizon' in order to accommodate varying time delays associated with each measurement in relation to the IMU. The data from each sensor is stored in a First-In-First-Out (FIFO) buffer and subsequently accessed by the EKF at the appropriate moment. The utilization of a complementary filter facilitates the progression of states from the designated 'fusion time horizon' to the present time by employing the buffered IMU data. This filter can be denoted as:

$$FM_{filtered,k} = az_k + (1+a)IMU_{filtered,k} \tag{40}$$

where $FM_{filtered,k}$ is the filtered and aligned measurement, $IMU_{filtered,k}$ is the filtered IMU measurement, and a is a weighting factor, often determined based on the characteristics of the sensors and the desired filter response.

The adjustment of the position and velocity states takes into consideration the offset between the IMU and the body frame prior to their output to the control loops. Moreover, distance sensors are employed to gauge the distance between the vehicle and the nets, achieving a range resolution of approximately 1 cm. To achieve that it moves respectively forward or backwards. A simplified model is given as follows:

$$U_d = \frac{1}{2}(sign(d-a) + sign(d-b)) \bullet m \tag{41}$$

where U_d is the control output speed, d the input distance from the sensor, m the motor control output multiplier, and a and b the minimum and maximum thresholds.

More specifically, the vehicle inspects the cubic net cages horizontally and changes depth following each round. It initiates its operation by commencing from a predefined initial location based on the data obtained from its magnetometer, and each round includes movement in a parallel manner to the net, exhibiting a swaying motion, while maintaining a constant distance of approximately 90–150 cm from the net. When it reaches a corner, it turns 90 degrees and continues its movement. Upon completing a full round, it descends by a distance of 1 m and iterates in the same manner until the predetermined maximum depth.

4.4.2. Trajectory tracking

What is more, the path following control system is based on the Line-Of-Sight (LOS) guidance law and applied in a similar rationale as in (Amundsen et al., 2021). To simplify the models, we considered a 2-D desired path P in C^2, as the vehicle is moving sideways with the depth controlled by the Pixhawk, parameterized as $p_\theta = (x_p(\theta), y_p(\theta))$, and θ is the variable representing the path. The system should ensure that the vehicle follows the path P with specified speed U_d while also ensuring that the heading angle converges to a desired heading ψ_d. For any p_θ across P, the path-tangential reference frame is rotated by the path-tangential angle about the north-east reference frame as follows:

$$\gamma_p(\theta) = atan2(y_p'(\theta), x_p'(\theta)) \tag{42}$$

In addition, the crosstrack error represents the distance from a location to the path-tangential reference frame, measured orthogonally as follows (Amundsen et al., 2021):

$$y_e(\theta) = -(x - x_p(\theta))\sin\Big(\gamma_p(\theta)\Big)\cos(\gamma_p(\theta)) \tag{43}$$

The LOS guidance law relies on the computation of a course angle (X_{LOS}), which, if accurately followed, will result in path following characteristics. This course angle is determined as follows, using Δ as the lookahead distance, which is a positive constant:

$$X_{LOS} \triangleq \gamma_p - \arctan(\frac{y_e}{\Delta}) \tag{44}$$

Fig. 8 visualizes the trajectory of an inspection operation inside a net cage 7x7 with 3.5 m depth for one lap (2D). These data were attained from distance sensors and IMU.

5. Results

5.1. CFD Simulation

Prior to conducting experiments with Kalypso in real environment, it was essential to comprehend the drag forces that are exerted on the vehicle during its movement. This is feasible through the determination of the hydrodynamic coefficients using CFD simulations. The parameters used for the CFD simulation are presented in Table 2.

Table 2
Physical and geometrical parameters.

Vehicle parameter	Value
Mass (m)	12.3 kg
Acceleration of gravity (g)	9.8 m/s^2
Density of water (ρ)	1026 kg/m^3
Volume of fluid displaced (∇)	0.01851 m^3
Center of gravity (r_g)	$[x_g\ y_g\ z_g] = [0, 0, 0]$
Center of buoyancy (r_b)	$[x_b, y_b, z_b] = [0, 0, 0]$

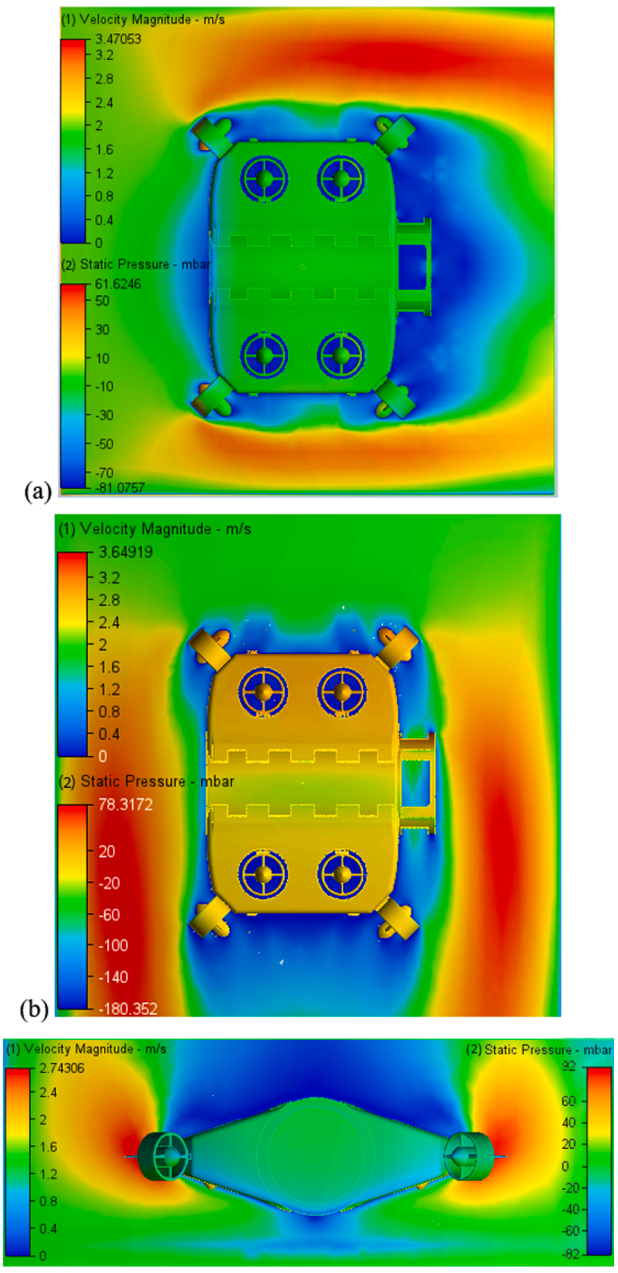

Fig. 9. Visualization of the HROVs CFD simulation water flow: *(a)* Surge motion simulation of forward movement, *(b)* Sway motion simulation of lateral-right movement, *(c)* Heave motion simulation of descend.

Kalypso is designed for deployment in seawater and is subject to specific performance parameters. The maximum impact velocity of the water on the vehicle is dependent on its speed and movement, with a limit of 2 m/s for the surge and sway motions and 1 m/s for the heave motion. Fig. 9 presents a visual representation of the water flow and the pressure on the vehicle derived from the CFD software. More specifically, the fluid is contingent on the scale "(1) Velocity Magnitude" presented in Fig. 9, which is the speed of the water around the vehicle in m/s, while the scale "(2) Static Pressure" pertains to the pressure on the skin of the vehicle in mbar.

The simulation results demonstrate that there is an overall force of *(a)* 121.97 Newtons exerted on surge, *(b)* 74.06 Newtons exerted on sway, and *(c)* 162.19 Newtons exerted on heave, while the drag coefficient values of 0.853, 0.518, and 2.

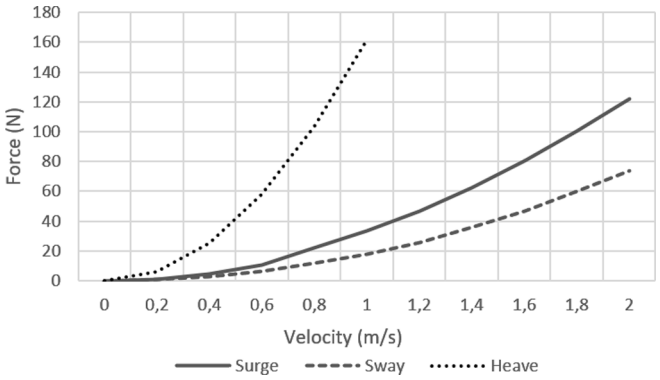

Fig. 10. Simulation results: Force imparted on the vehicle related to its speed for each axis movement.

The hydrodynamic configuration of Kalypso's architectural design yields enhanced efficiency in sway motion, as anticipated. The vehicle's heave motion is distinguished by an elevated drag coefficient, leading to enhanced stability while traversing through net cages, albeit at the cost of impeding its motion. Furthermore, as depicted in Fig. 9 (b), it is visible that the vehicle encounters greater amounts of uniform pressure on its upper (and lower) regions in contrast to the other two movements. The surge motion results in higher values on the front, while the heave motion leads to cumulative force on the upper and lower parts.

Under the evaluation of hydrodynamic performance, the flow simulation provides valuable insights into the vehicle's behavior and performance in water, including the forces acting on it. It helps in understanding the vehicle's maneuverability, stability, and efficiency by analyzing factors such as drag coefficients and overall flow characteristics around the vehicle. Thus, it is interesting to examine the forces acting on the vehicle on all three axes at different speeds and the related drag coefficient. Fig. 10 plots the force imparted on the vehicle related to its speed for each translational movement.

The detailed results for each simulation that are visualized in Fig. 10 are quoted in Table B1 in Appendix B.

Furthermore, the forces acting on the three tool manipulators had to be investigated, and therefore a CFD simulation was conducted. The results are quoted in Table 3. (see Tables 4 and 5).

Table 3
Moments of all thrusters in meters (m).

T_i	l_{xi} (m)	l_{yi} (m)	l_{zi} (m)
T_1	0.16	0.248	0
T_2	0.16	−0.248	0
T_3	−0.16	0.248	0
T_4	−0.16	−0.248	0
T_5	0.07	0.161	0
T_6	0.07	−0.161	0
T_7	−0.07	0.161	0
T_8	−0.07	−0.161	0

Table 4
Parameters of the CFD Simulation.

Parameter	Value
Fluid	Sea Water
Density of Fluid	1.0212 g/cm^3
Velocity	2 m/s (1 m/s on heave)
Iterations	100

Table 5
Forces and drag coefficients of the 3 manipulators in 3 translational motions.

Tool Manipulator	Surge		Sway		Heave	
	Force (N)	Drag Coefficient	Force (N)	Drag Coefficient	Force (N)	Drag Coef.
Object gripper	5.35	0.4352	13.9	0.484	19.7	0.685
Fish mort grabber	18.03	0.7426	49	1.066	35.743	1.037
Net tear repairing	1.5	0.1012	1.85	0.28	7.3	0.25

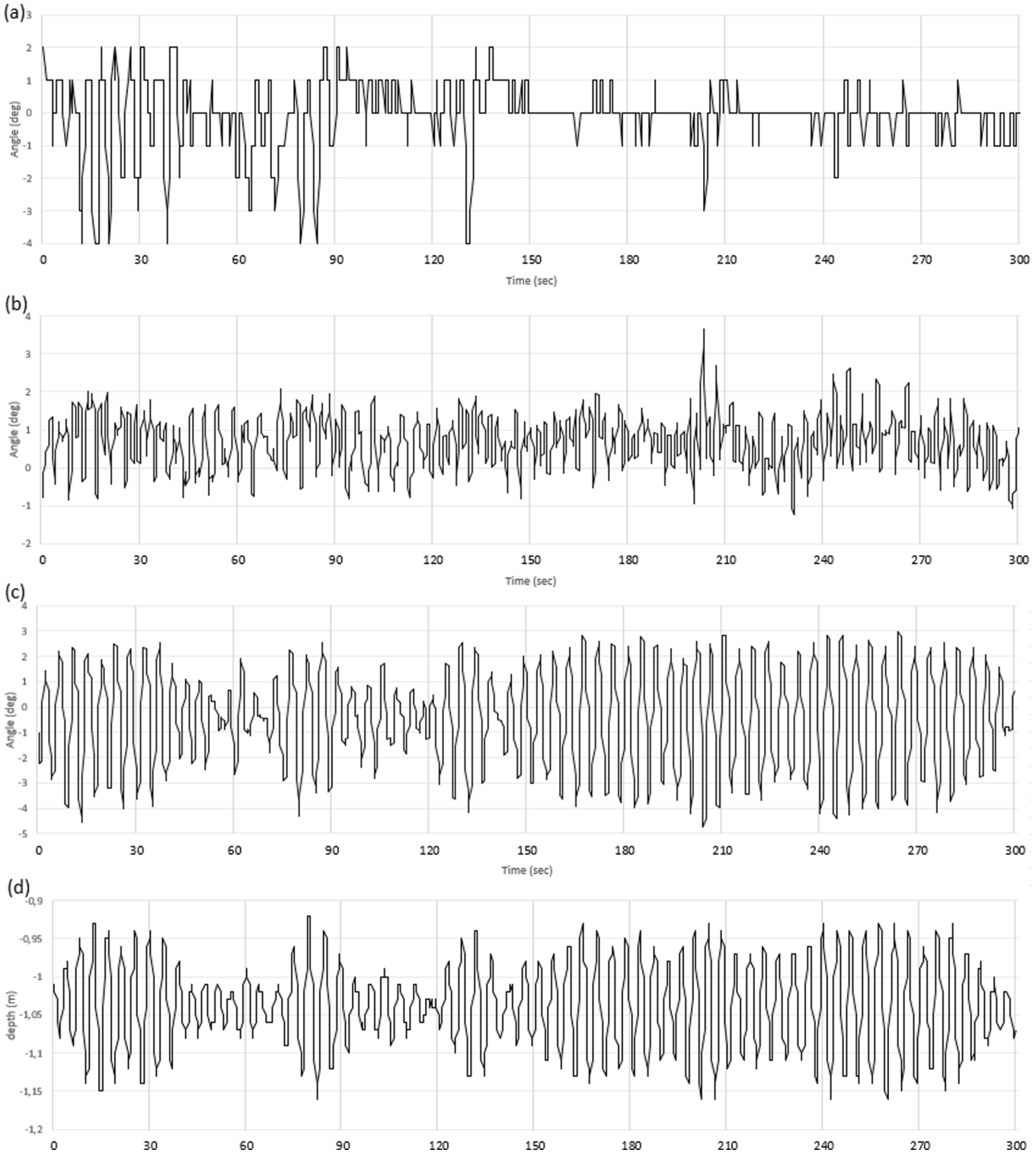

Fig. 11. Sensor values on depth hold mode for 5 min: *(a)* Yaw, *(b)* Roll, *(c)* Pitch, *(d)* Depth.

5.2. Mission performance – field experiments

5.2.1. Field trial information

Field trials were undertaken in fish farms located in Kefalonia, Greece. All testing occurred within the net cages of the fish farm housing sea bass. The net cages measure 7 m in length, 7 m in width, and 10 m in depth. The net cages were situated approximately 80 m offshore.

The HROV has been developed for employment in marine environments, particularly in seawater, and has a maximum operational depth of 10 m, corresponding to the depth of the net cages at the Kefalonia fish farms. The components of the system have been certified to withstand submersion up to 100 m. However, due to the unavailability of resources to conduct experiments at such depths, the maximum depth tested was approximately 17 m.

The field experiments presented are as follows:

i. Stationary and rotational test to evaluate stability
ii. Autonomous movement evaluation and testing
iii. Manipulator experimentation

5.2.2. Stationary and rotational test

The examination of the three rotational movements (yaw, pitch, and roll) plays a critical role in ensuring the stability and controllability of underwater vehicles operating in dynamic and sometimes unpredictable environments, such as aquaculture. Stability is particularly essential to maintain precision in operations, avoid unnecessary energy consumption, and ensure the longevity of the vehicle's operational capabilities.

In this study, the vehicle was submerged to a depth of 1 meter (m) while being operated in depth hold mode, which is designed to maintain a fixed depth despite external disturbances. The depth hold mode leverages advanced control algorithms integrating feedback from onboard sensors to stabilize the vehicle's position and orientation. By evaluating the rotational deviations—yaw, pitch, and roll—the study aimed to assess the effectiveness of the control systems in mitigating external perturbations that commonly occur due to water currents or turbulence.

The results demonstrated that the vehicle's stability in the underwater environment was commendable, with maximum rotational deviations of 4.0°, 4.1°, and 3.6° in yaw, pitch, and roll, respectively. These values indicate that the integrated control system successfully managed to suppress significant oscillatory behavior, keeping the vehicle's orientation within acceptable bounds for operations at shallow depths. The recorded depth measurements ranged from −0.91 to −1.16 m. This slight fluctuation reflects the vehicle's ability to respond to disturbances while maintaining an overall mean depth close to the target value of −1.0 m. Such a performance highlights the depth hold mode's reliability under typical operational conditions.

Fig. 11 provides a comprehensive visualization of these rotational movements and depth variations over a 5-minute measurement period. Panel (a) illustrates yaw deviations, showing rapid adjustments to maintain stability. Panel (b) depicts pitch deviations, indicating the control system's responsiveness to vertical perturbations. Panel (c) represents roll deviations, which demonstrate the vehicle's robustness against lateral tilt. Lastly, panel (d) showcases depth variation over time, further reinforcing the vehicle's capacity to sustain a steady operating depth. Together, these visualizations underline the system's integrated stability performance.

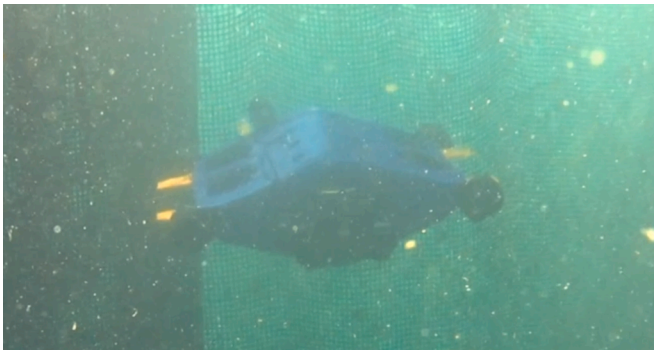

Fig. 13. Photograph capturing Kalypso during autonomous operation.

These results are significant for operations in fisheries aquaculture where precision and stability are paramount to avoid disturbances to the aquatic ecosystem. The vehicle's demonstrated stability ensures it can perform delicate tasks, such as monitoring and intervention, without causing unnecessary stress or disruption to marine life.

In addition, the power consumption of the thrusters in the same 5-minute measurement was recorded and is presented in Fig. 12. The plot visualizes the power draw of the thrusters in Amperes (A) per second. The total estimated power consumption of this 5-minute test was about 0.2664 Ampere Hours (Ah).

Empirically, the vehicle's endurance is about 3–5 h on a typical use depending on the mission.

5.2.3. Autonomous movement evaluation and testing

The vehicle underwent testing in its autonomous mode without the need for a tether. It conducted tetherless autonomous navigation inside a square net cage in order to record video (Fig. 13). To evaluate the performance of the vehicle for net cage inspection, an experiment was conducted in a square net cage with dimensions of 7x7 meters and a depth of 3.5 m and a total area of 98 m^2. The objective of the experiment was to evaluate Kalypso's capability to capture the yellow rectangular labels that were positioned randomly inside the net cage.

Preceding the experimental procedure, a diver placed 10 rectangular

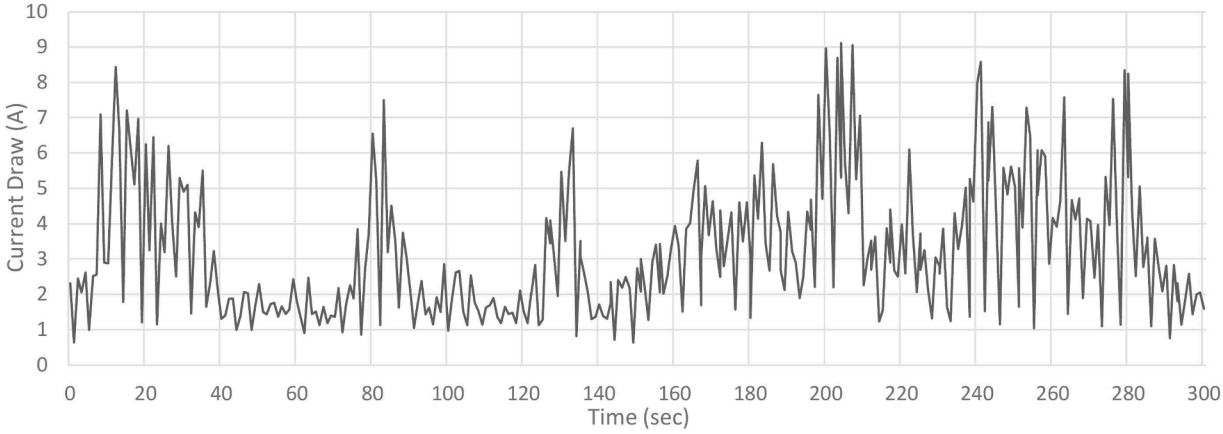

Fig. 12. Current draw of the thrusters.

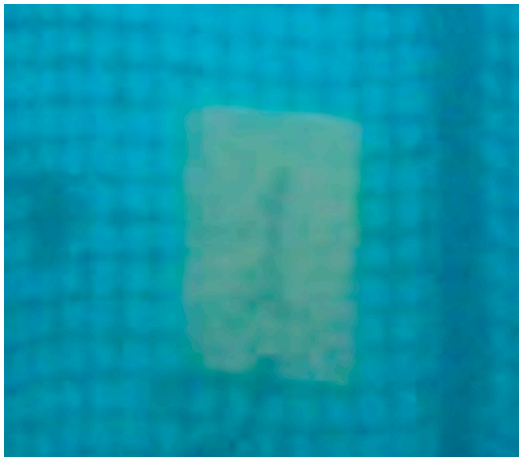

Fig. 14. Example of an image of the captured label.

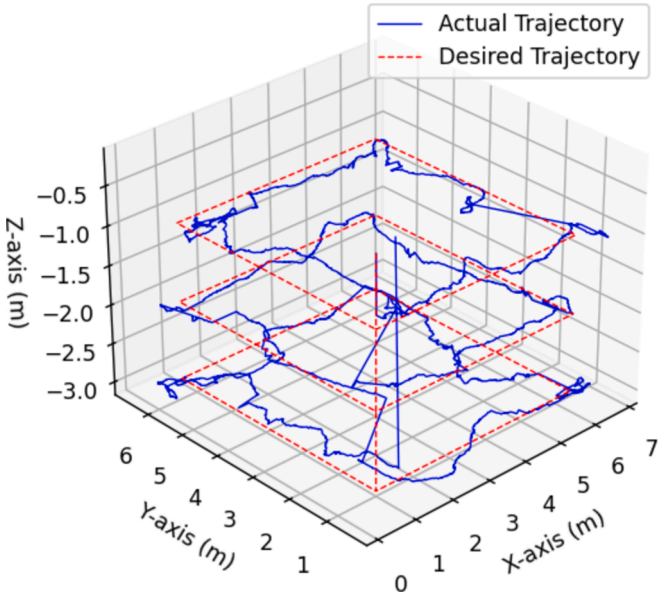

Fig. 15. Trajectory tracking in real conditions inside a fish net cage.

labels of yellow color at diverse locations inside the net enclosure. The concept of the labels was aimed at emulating objects of interest (net tears) that the HROV was required to record in the course of its inspection. The color of the labels was chosen in order to be highly visible to the camera. Also, the labels were numbered from 1 to 10.

The AUV was then deployed in autonomous mode to record the visual content of the net cage during the inspection process. The primary objective of the mission was to capture all 10 yellow labels within the net cage. The efficacy of the mission was ascertained by the quantity of the labels that were captured by Kalypso.

The task commences with the operator initiating the vehicle and submerging it into the net cages. The vehicle's orientation is meticulously set to face one side of the nets, with the right side of the vehicle precisely aligned with the other side of the nets (90°), maintaining a consistent distance ranging from 60 to 120 cm from each side. Integration of a pressure sensor within the vehicle configuration serves also the purpose of detecting deployment; specifically, the system is programmed to activate once it detects a submersion depth of 0.2 m. Consequently, upon positioning the vehicle at the designated starting point, the operator is required to submerge the vehicle to a depth of 0.2 m, thereby triggering the initiation of its operational sequence. Subsequent to this activation, the vehicle embarks on the prescribed navigation trajectory within the net cage, as elucidated in Section 4.4. In particular, the vehicle records its initial orientation using the magnetometer (compass), then it gets submerged to 1 m depth. Subsequently, it systematically moves throught the cubic net cages horizontally, adjusting its depth after each round. Throughout each round, the vehicle executes parallel movements to the net, characterized by a swaying motion, while consistently upholding a fixed distance of around 90–150 cm from the net cages. At each corner encounter, the vehicle executes a precise 90-degree turn before resuming its course. Upon completing a full circuit, the vehicle descends by 1 m and reiterates the process until the designated maximum depth is reached.

During the inspection, the AUV navigated through the net cage, utilizing its sensors and onboard algorithms to capture the yellow labels. The AUV's video feed captured the entire inspection process, allowing for subsequent analysis and verification of label detection.

Upon concluding the inspection, the recorded visual media was reviewed and evaluated. The video frames that were obtained were reviewed to ascertain the quantity of yellow labels that were effectively detected by the AUV. The efficacy of the mission was determined by computing the proportion of located labels to the overall quantity of labels that were deposited inside the net enclosure. The experimental outcomes evinced the success of the developed AUV for the purpose of inspecting net cages. All ten yellow rectangle labels were successfully located and captured by the AUV, resulting in a 100 % success rate for the mission, exceeding our expectations. Regarding the label numbering, seven out of ten labels had their numerical values identified, while the numbers of the other three could not be discerned due to the blurred quality of the image. The capture of all the labels validates the AUV's ability to efficiently execute subaquatic inspections in order to detect points of interest within net cage environments. Fig. 14 is an example of the captured labels.

Moreover, the 3D trajectory plot presented in Fig. 15 illustrates the navigation and inspection capabilities of the underwater vehicle within the confined space of net cages measuring 7x7 meters up to 3 m in depth as described in the mission deployment above. The blue trajectory represents the actual path taken during inspections, showcasing the vehicle's ability to navigate through complex underwater environments. Meanwhile, the red dashed trajectory, depicting the desired path, highlights the planned trajectory for comparison. This visualization not only demonstrates the efficacy of the proposed underwater vehicle in performing inspections but also emphasizes its capability to adhere to predefined paths within the specific constraints of net cages and environmental impediments, such as fish and water currents. The data presented in Fig. 15 were captured using the distance sensors (sonars), the onboard IMU and the pressure sensor.

5.2.4. Manipulator experimentation

The vehicle underwent testing as a tethered manual vehicle that was operated by an individual who conducted inspections of the nets using semi-automatic motions. These encompass stabilize mode, which is designed to sustain the vessel's heading, and depth hold mode, which represents an advanced iteration of the stabilize mode by preserving the current depth. Furthermore, the combination of the vehicle and the tool manipulators in addressing the removal of objects, disposal of fish morts, and stitching of torn nets was performed in these manual operations. More specifically:

i. Object Removal and Fish Mort Disposal: The operation of these tools is simple and were tested in net cages to remove objects and collect fish morts. Kalypso demonstrated a high degree of maneuverability and stability during these trials, enabling the manipulator to effectively perform its functions despite having only one DoF. While the manipulator itself is relatively simple, its functionality is amplified by Kalypso's ability to precisely control its positioning and movement. By taking full responsibility for the vehicle's motion, Kalypso

Fig. 16. Photograph of the vehicle with the three manipulator tools integrated.

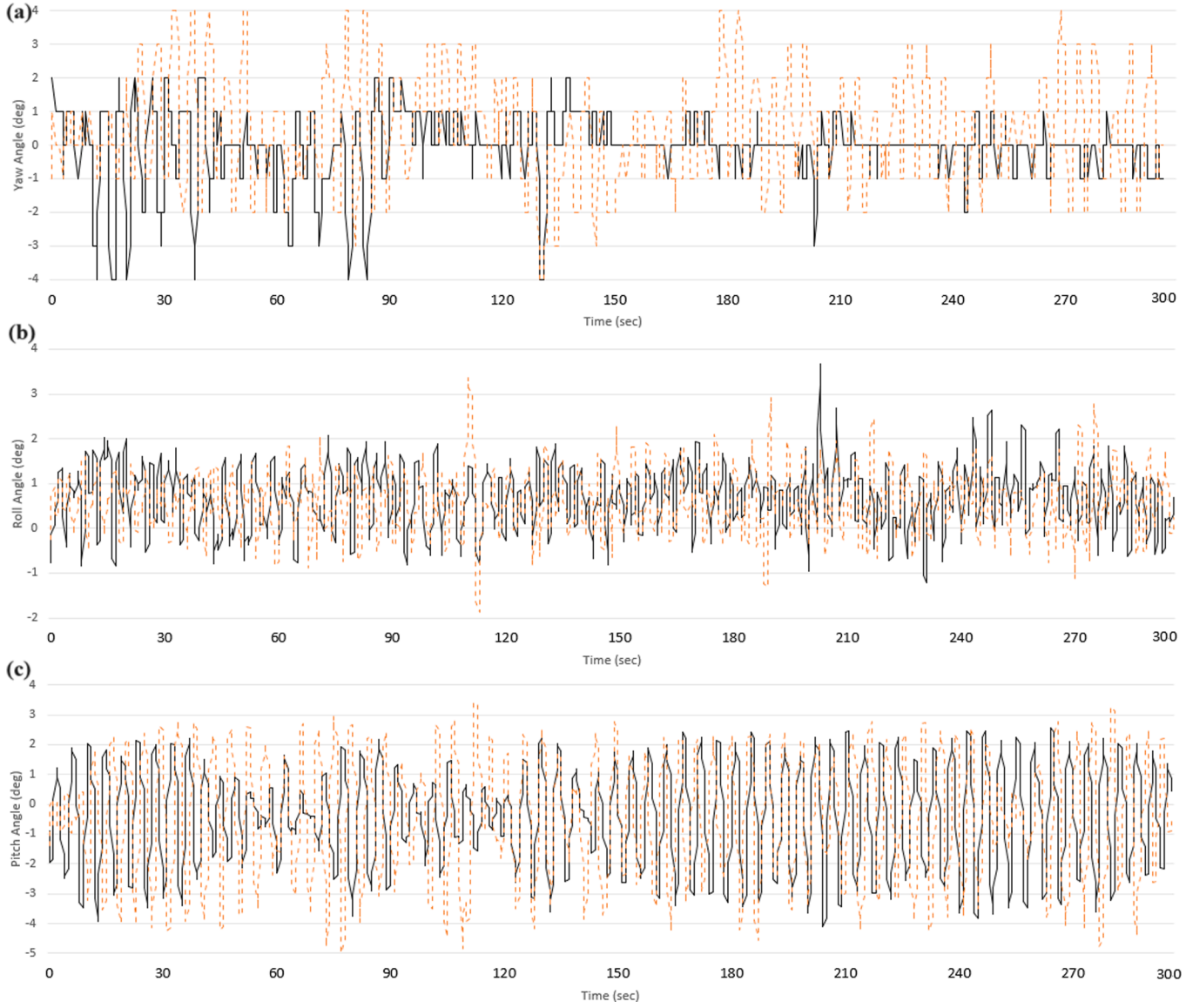

Fig. 17. Sensor values to assess vehicle stability before and after the integration of the manipulator: (a) Yaw, (b) Roll, (c) Pitch.

eliminates the need for additional arm-mounted DoF, streamlining operations and simplifying the system's design.

ii. Net Tear Stitching: The stitching of torn net sections represents another critical task, essential for maintaining the integrity of aquaculture enclosures and preventing the escape of fish stocks. The experimental evaluation involved deliberate perforation of net sections, followed by the repair of these holes using the manipulator. The operator played a pivotal role in guiding the vehicle to the location of each tear and executing the stitching process. The total time required for each stitching operation varied, influenced by

Table 6
Peak values and average deviations from a 5-minute stability test.

Motion	HROV	HROV & Arm	Difference
Yaw average	0.5768	−1.2573	0.6805
Yaw peak	2 | −4	4 | −4	2 | 0
Roll average	0.8	0.7328	−0.0672
Roll peak	3.66 | −1.22	3.366 | −1.877	−0.294 | 0.657
Pitch average	1.4	−1.7376	0.3376
Pitch peak	2.562 | −4.1	3.4 | −5.004	0.904 | 2.496

factors such as operator skill, weather conditions, and the complexity of the task. The subprocesses performed to complete the net repair involved (i) the hole identification and targeting, (ii) caliper placement, (iii) the locking and engagement, and (iv) the detachment.

The vehicle was placed inside the net cages and was tested as a tethered remotely operated vehicle using the depth hold mode. For each operation, the appropriate tool manipulator was attached prior to the operation.

Currently, the successful completion of all experimental procedures requires the involvement of an operator to carry out the designated tasks. The vehicle exhibits consistent stability across various pitch angles, allowing the manipulators to effortlessly grab both stationary and moving targets in any given orientation. For example, if fish morts are detected floating on the surface of the ocean, it is necessary for the vehicle to perform a rotational movement along its transverse *(Y)* axis in order to align itself with the surface. In general, it can ensure stability across all rotations, thus facilitating the operational functionality of the manipulators in various orientations. The amount of time needed to finish each task can vary greatly depending on a number of factors, including the operator's degree of expertise, the environmental conditions, and the specifics of the problem that needs to be solved. For instance, the procedure of capturing deceased fish generally necessitates an estimated duration of 30 s, encompassing the initial targeting stage up until the actual capture. Similarly, repairing tears in a net requires around 70 s, including the steps of identifying the tear and then detaching it. In Fig. 16, three photographs of the vehicle with the tool integrated are quoted.

The evaluation of the vehicle's stability extends to the scenario with the integration of the underwater manipulator in order to compare and discern deviations in performance. Fig. 17 plots the results, facilitating a nuanced examination of stability both with and without the attached underwater manipulator. The ensuing numerical disparities invite a meticulous scrutiny of the vehicle's behavior under these distinct operational configurations. More specifically, it was observed that the differences between the average values of the deviation of the rotational axes are insignificant except on the yaw, which exhibits the highest deviation with a 0.68° difference. The full list of results, including the peek values and the average deviation values are quoted in Table 6.

6. Discussion

6.1. Key insights

The implementation of the Kalypso within the Kefalonia fish farms provided an opportunity to glean valuable insights that bridge the realms of underwater robotics and aquaculture management.

A fundamental insight gained from this endeavor was the significance of tailoring technological solutions to the specific needs and conditions of the operational environment. The distinct challenges posed by Kefalonia's marine ecosystem, including fluctuating currents and varying maintenance tasks, illuminated the importance of adaptability in HROV's design and behavior. On-site adjustments, configurations, and refinements are essential to ensure the vehicle operates effectively for the assigned tasks.

Furthermore, the vehicle's implementation underscored the real-world validation. By immersing the HROV in operational aquaculture environments, this research transcended the realm of simulation and substitute environments (e.g. water tanks), generating authentic data that refined our understanding of aquatic dynamics compared to the simulation ones. The pragmatic environment, including external factors such as currents, waves, and fish, is quite distant from the domain of simulation and modeling. For instance, it was observed that the fish maintained a consistent distance of 1.5 to 2 m (visual estimation) from the robot, allowing the distance sensor to function flawlessly. However, some false values from fish reflections were distinct and filtered. Moreover, the observation of such fish response aligns with the findings of the literature which highlights the potential of tailored underwater robots to enhance fish monitoring practices (Kruusmaa et al., 2020). This paves the way for future design decisions about the HROV to be made with the intention of minimizing the negative impact on the fish.

In addition, the utilization of the underwater manipulator for maintenance purposes endeavors to foster the quality of the environment inside the net cage by increasing the frequency of fish mort disposal and reduce fish loss by repairing net tears. In light of this, this research also highlights the paramount significance of interdisciplinary collaboration. The synthesis of engineering expertise with the nuanced insights of marine biologists and aquaculture experts demonstrated the transformative potential of cross-disciplinary partnerships in order to increase the quality and fish welfare.

Lastly, the study emphasized the ongoing nature of technology deployment in real-world settings; Kalypso's presence in aquaculture underscored that continuous monitoring, maintenance, and refinement are integral to sustaining the benefits of such systems for long-term aquatic resource management. The deployment in Kefalonia also emphasized the significance of engaging with aquaculture's stakeholders, including divers and fish feeders, whose insights not only enriched our understanding but also established a sense of shared responsibility towards ecosystem preservation.

6.2. Limitations of the proposed solution

The development of any complex technological solution inherently comes with its set of challenges and constraints. These limitations encapsulate the intricate interaction between technological capabilities and the complexities of underwater environments. By comprehensively understanding and acknowledging these limitations, a transparent assessment of the system's operational boundaries is provided. Through a clear elucidation of these constraints, the way is paved for future advancements and refinements, ensuring that the system's potential impact is optimized. The limitations of the system are listed as follows:

- *Communication when tetherless*: As the underwater vehicle operates autonomously in an underwater environment without a tether, communication with the vehicle is absent. Thus, the vehicle cannot send visual feedback or receive commands. Technical solutions such as acoustic or optical modems could provide bilateral communication if the fish do not disrupt this communication. Nevertheless, the utilization of such systems entails a substantial expense that may surpass the cost of the vehicle.
- *Limited sensory perception*: While the underwater vehicle system is equipped with sensors to perceive its surroundings, the sensors might have limitations in accurately detecting certain underwater features, leading to potential navigation inaccuracies. Investing in higher-priced equipment has the potential to enhance undersea operations.
- *Interference with fish*: The underwater vehicle is employed within the fish net cages. Thus, the fish can be recognized as – moving – obstacles by the distance sensors. To mitigate this phenomenon, some filters were applied, neglecting specific values.
- *Data processing limitations*: The system has a mini-PC that can process a large amount of data. However, its capabilities are not limitless.

This processor is capable of executing computer vision algorithms, although its effectiveness may vary depending on the specific scenario.

- *Complexity of manipulation*: While the underwater manipulator's capabilities are designed to enhance the system's functionality, manipulating objects underwater can be challenging due to the three-dimensional nature of the underwater space and the varying environmental conditions.
- *Torque limitation of the tool manipulator*: The underwear manipulator is actuated by a single servo motor to achieve cost-effectiveness. Therefore, its torque capacities are limited but sufficient for the maintenance needs of aquaculture. Utilizing more sophisticated motors could enhance its overall force.
- *Inefficient in heave motion*: The vehicle is intentionally designed to have increased resistance to vertical motion, which enhances its stability. However, if the vehicle is required to undergo prolonged heave motion, its effectiveness would be lowered.
- *Power and endurance*: The vehicle operates using LiPo batteries. Consequently, its operating endurance is limited.
- *Skill requirements*: Operating and maintaining the proposed underwater vehicle system demands basic knowledge about the vehicle and its features. This necessity will diminish if the vehicle acquire greater autonomous functionalities.
- *Calibration and alignment*: The accurate operation of the system's manipulators and sensors relies on precise calibration and alignment. Calibrating the system requires specialized procedures and could be prone to errors.
- *Deployment and retrieval*: Launching and retrieving the underwater vehicle system, especially in challenging weather conditions, might pose operational difficulties.
- *Maintenance*: In order to ensure optimal vehicle performance, it is imperative to rinse it thoroughly with clean water following usage. Alternatively, it may lead to a decrease in life expectancy.

6.3. Benefits of underwater vehicles in aquaculture

Underwater robotic systems have become useful tools for the aquaculture industry and introduce several benefits that improve production efficiency, environmental sustainability, and cost-effectiveness (Kitowski and Soliński, 2016). The deployment of such systems facilitates enables a transformation in conventional aquaculture practices, introducing in a new era of precision and automation.

One of the primary advantages lies in the realm of cost mitigation. UUVs negate the need for human divers, thereby minimizing labor costs associated with routine inspections, maintenance, and data collection (Wu et al., 2022). This economic efficiency extends further to limiting expenditures linked to diver training, safety protocols, and health insurance. The financial viability of aquaculture endeavors is thereby augmented, fostering a more sustainable economic model. Moreover, the application of underwater robotic systems in aquaculture yields benefits beyond the immediate realms of cost-effectiveness. A critical facet lies in the enhancement of safety protocols and risk mitigation within aquaculture facilities (Brandt et al., 2023). By relegating hazardous tasks to robotic vehicles, the potential exposure of human divers to perilous conditions, such as adverse weather, strong currents, or

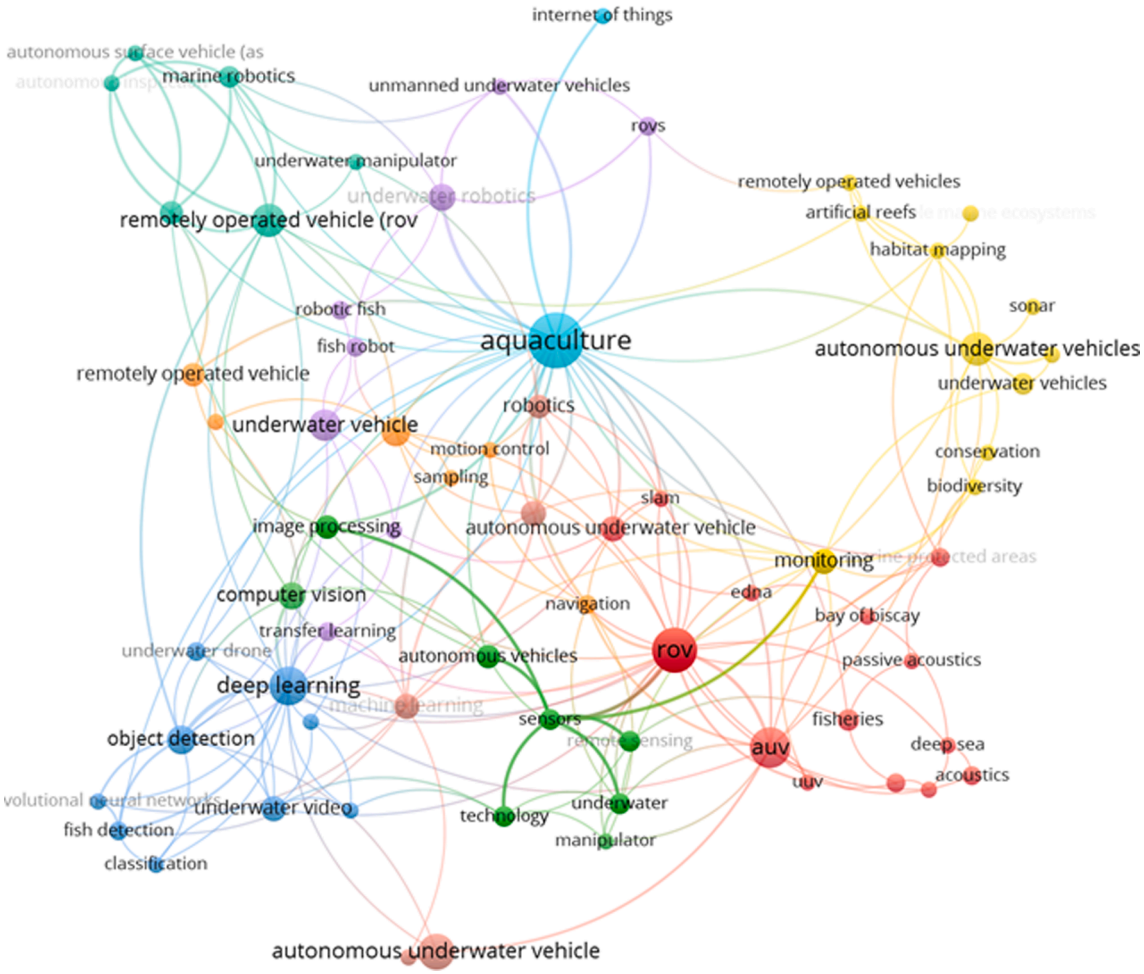

Fig. 18. Visual representation of the keyword relationships regarding underwater robotics and aquaculture.

contaminated waters, is significantly diminished. This prioritization of safety not only safeguards human lives but also mitigates operational disruptions that may arise from unpredictable environmental factors.

Furthermore, the integration of underwater robotic systems in aquaculture operations engenders increased levels of environmental stewardship. The decrease in human involvement results in a reduced carbon footprint, indicating a dedication to environmentally sustainable methods. (Rowan, 2023). This commitment to eco-friendly methodologies aligns with broader imperatives for sustainable resource management and resonates with contemporary paradigms of responsible industrial conduct (Kyrgiakos et al., 2023). Additionally, the implementation of underwater technologies facilitates monitoring of environmental variables, such as water quality and temperature, thereby enabling prompt responses to potential anomalies and ensuring optimal conditions for aquatic life.

Moreover, the advent of underwater robotic manipulators introduces a transformative dimension to aquaculture practices. These systems, equipped with advanced sensory and dexterous capabilities, can perform intricate tasks, including biofouling prevention (Ohrem et al., September 2020), net cleaning (Fu et al., 2024), and even underwater repairs. Such versatility not only enhances the overall efficiency of aquaculture operations but also extends the operational lifespan of infrastructure (Ferreira et al., 2018), reducing the need for frequent replacements.

In the context of data acquisition and analytics, underwater robotic systems serve as invaluable tools for researchers and aquaculturists alike (Al-Hussaini et al., 2018). Equipped with a suite of sensors, these systems can collect comprehensive datasets encompassing parameters such as water chemistry (Simbeye and Yang, 2014), biomass measurements (Santos-Ballardo et al., 2015), and environmental conditions (Wu et al., 2022). The synthesis of this data not only empowers aquaculture practitioners with actionable insights for informed decision-making but also contributes to the broader scientific understanding of aquatic ecosystems.

In conclusion, the integration of underwater systems in aquaculture heralds a transformative era marked by heightened efficiency, environmental responsibility, and technological innovation. These systems, ranging from ROVs to AUVs and supportive manipulators, collectively redefine the landscape of aquaculture operations, propelling the industry towards sustainable and technologically driven practices.

6.4. Future trends of underwater vehicles in aquaculture

In the pursuit of comprehending the intricate research landscape within the aquaculture and underwater robotics domains, a sophisticated bibliometric analysis was conducted employing VOSviewer (Waltman and Ecken, 2010). This type of analysis can help identify clusters of related keywords, highlight emerging trends, and reveal the interconnectedness of different research areas within a specific field. The data ware extracted from the Scopus database using the terms "*underwater robotics*" or "*underwater vehicle*" and "*aquaculture*" or "*mariculture*" or "*fisheries*" in titles, abstracts, and keywords and fed into VOSviewer. The full query is given in Appendix C. Through the meticulous examination of keyword co-occurrence, this approach revealed a nuanced interaction of ideas and concepts across the scholarly landscape. The resulting visual representation encapsulates the synergies and interconnections between keywords, offering a holistic perspective on the evolving trends and focal points in the field (Fig. 18). This method not only serves as a navigational tool through academic literature but also unveils future trends and relationships that may elude traditional analyses. The intricate network of keywords, meticulously unveiled by VOSviewer, thus stands as a testament to the dynamic nature of research in underwater robotics applied to aquaculture, providing a foundation for future exploration and scholarly inquiry. By visually examining the network of keywords and the cluster results, it can be concluded that eight clusters were created regarding underwater robotics as follows: *(i)* ROV – marine robotics – underwater manipulator – autonomous surface vehicle, *(ii)* underwater vehicle – ROV – fish robot – underwater robotics UUVs – navigation – motion control – sampling, *(iii)* deep learning – object detection – underwater video – fish detection – computer vision, *(iv)* sensors – remote sensing – underwater – image processing – computer vision, *(v)* AUV – machine learning – path planning – robotics, *(vi)* ROV – AUV – UUV – fisheries – acoustics, *(vii)* AUVs – underwater vehicles – ROVs – monitoring – biodiversity – conservation – habitat mapping, *(viii)* aquaculture – internet of things. Thus, this section is driven by these clusters.

6.4.1. Confluence with artificial intelligence

The future trajectory of underwater robotic systems within the aquaculture industry is poised to witness a confluence of advancements that transcend the current technological landscape. Foremost among these anticipated trends is the integration of Artificial Intelligence (AI) and Machine Learning (ML) algorithms into robotic functionalities (Mandal and Ghosh, 2023). This infusion of cognitive capabilities is anticipated to imbue underwater robotic systems with increased autonomy and adaptability (Skaldebø et al., 2023). By endowing these systems with the capacity to learn from environmental dynamics and aquaculture operations, they are expected to evolve into intelligent entities capable of nuanced decision-making and the optimization of operational parameters. In light of this, the overall efficacy and autonomy levels of the proposed system could be enhanced through the implementation of intelligent functions.

6.4.2. Advancements in navigation systems

Furthermore, anticipated advancements in navigation systems are poised to incorporate state-of-the-art sensor arrays, leveraging innovations in computer vision, LiDAR, and acoustic technologies (Xie et al., 2023). This integration will empower underwater vehicles with an enhanced ability to perceive and navigate complex aquaculture environments with a level of dexterity mirroring natural aquatic organisms. Moreover, motion control systems are slated to undergo a paradigm shift towards increased autonomy and adaptability (Sitler and Wang, 2022). Machine learning algorithms and artificial intelligence will play pivotal roles in endowing underwater vehicles with the capacity to learn and adapt their motion strategies based on environmental cues and historical data. In addition, the fusion of navigation and motion control technologies is envisioned to facilitate swarm robotics applications, wherein multiple underwater vehicles collaborate seamlessly to accomplish tasks with efficiency and precision. This aligns with the limitations of the proposed solution, as future endeavors will augment sensory perception and enable enhanced navigation capabilities, minimizing the operator's skill requirements.

6.4.3. Evolution of underwater sensors

Parallelly, miniaturization and the development of more compact yet potent sensor arrays are anticipated to redefine the form factor and sensing capabilities of underwater robotic systems (Biazi and Marques, 2023). This trend aligns with the imperative for unobtrusive yet comprehensive monitoring within aquaculture facilities (Brandt et al., 2023). Miniaturized sensors, characterized by enhanced precision and sensitivity, hold the promise of facilitating more granular data collection, enabling researchers to glean insights into subtle changes within the aquatic environment. Next-generation underwater vehicles are poised to leverage a fusion of sensor types, including but not limited to vision-based sensors, acoustic sensors, environmental sensors, and biological sensors (Wu et al., 2022; Ji et al., 2023). This amalgamation is geared towards endowing these vehicles with a comprehensive understanding of the aquatic environment, encompassing water quality parameters, marine life behavior, and structural nuances of aquaculture facilities. Vision-based sensors, driven by advancements in computer vision and machine learning algorithms, empowers underwater vehicles with robust object recognition capabilities (Liu et al., 2023). This

enables not only the precise identification of fish health, biomass, and potential anomalies but also the dynamic assessment of structural integrity within aquaculture infrastructure. Acoustic sensors, on the other hand, play a pivotal role in enhancing navigation and communication capabilities. Innovations in sonar technologies can contribute to improved underwater mapping, obstacle avoidance, and efficient communication between vehicles, thereby optimizing collective operations in swarm robotics.

6.4.4. Energy management, propulsion technologies, and human–machine interaction

Moreover, advancements in energy management and propulsion technologies are pivotal considerations for the future of underwater robotic systems (Lemos et al., 2021). Innovations in propulsion mechanisms, inspired by biomimicry and unconventional engineering paradigms, are expected to enhance maneuverability and operational versatility (Lamraoui et al., 2022). This is a significant issue as it delves into operational adequacy in specific tasks as outlined in the limitations of the proposed system. What is more, human–machine collaboration represents another frontier in the evolution of underwater robotic systems. The development of intuitive human–machine interfaces and teleoperation capabilities seeks to foster a symbiotic relationship between human expertise and robotic efficiency (D. Guihen, 2023). Since the operator's engagement with the proposed system necessitates deployment, retrieval, skill requirements, and operational interaction, boosting the quality of this interaction is essential. This collaborative model envisions aquaculturists working in tandem with robotic systems, leveraging the strengths of both to optimize decision-making and operational outcomes.

6.4.5. Steps towards industry 4.0

In conclusion, the future trends of underwater robotic systems in the aquaculture industry converge on the augmentation of intelligence, miniaturization, interconnectivity, energy efficiency, human–machine collaboration, and environmental resilience. Underwater vehicles equipped with advanced sensing capabilities and real-time data processing align seamlessly with the principles of Industry 4.0, fostering a cyber-physical ecosystem (Yue and Shen, 2022). These robotic systems, interconnected through the Internet of Things (IoT), can facilitate not only precise monitoring of aquatic environments but also enable intelligent decision-making (Biazi and Marques, 2023). The fusion of robotics, data analytics, and machine learning within aquaculture aligns with the tenets of Industry 4.0, promising increased efficiency, sustainability, and adaptability. As aquaculture ventures embrace this technological evolution, the sector is poised to achieve higher levels of productivity and environmental responsibility, marking a significant stride towards the future of smart aquaculture.

7. Conclusion

In brief, the present study analyzes an HROV utilized for the purpose of inspecting and maintaining net cages in aquaculture. The design of the vehicle incorporates six DoF, and rotational and translational velocities are deemed adequate for inspection purposes. The construction cost of the vehicle is 4050 euros, while the manipulator's is 30 euros. The safety of the vehicle is ensured by the presence of 3D-printed protective parts that cover its propellers. Additionally, the absence of any hazardous components on the vehicle's surface eliminates the possibility of accidents resulting from physical interaction with it. Furthermore, the high scalability and interoperability of the system are attributed to the open-source nature of its components as well as the high modularity of its hull. The primary impediment to the versatility and adaptability of most vehicles is the watertight enclosure, which necessitates the opening of seals for hardware modifications when switching between task operations. However, in this vehicle, appropriate plugs were installed that can change between different cables without opening the watertight enclosure. This offers on-site addition of sensors or the underwater tool manipulator. This also applies to the execution of maintenance activities.

The implementation of underwater robotic systems, as previously mentioned, offers significant benefits to the aquaculture industry. The deployment of these systems holds the promise of increasing productivity and efficacy while simultaneously reducing labor expenses and improving safety protocols. Aquaculture systems possess the capacity to improve the welfare and health of fish populations by enabling the effective removal of fish morts and expediting net tear repairs to net cages. However, the application of underwater vehicles in the field of aquaculture is not devoid of its own set of challenges and shortcomings. The costs associated with acquiring and maintaining underwater systems can be significant, and achieving their optimum performance may require specialized training. In light of the aforementioned challenges, it appears that the integration of the tool manipulator into Kalypso can enhance operational efficacy at Kefalonia fish farms and promote the well-being of the fauna through consistent interventions.

Further research efforts involve performing a range of tests on Kalypso alongside the tool manipulator incorporated into different automated procedures. In more detail, the vehicle's software will be enhanced by merging its computer vision capabilities with the use of the tool. Furthermore, the addition of a secondary manipulator to the vehicle could be beneficial in order to manipulate the nets when a tear is detected.

Funding

European Union and Greek national funds through the Operational Program Competitiveness, Entrepreneurship and Innovation, under the call RESEARCH – CREATE – INNOVATE (project code: T2EDK- 02504).

CRediT authorship contribution statement

Marios Vasileiou: Writing – review & editing, Writing – original draft, Visualization, Validation, Software, Methodology, Investigation, Formal analysis, Data curation, Conceptualization. **George Vlontzos:** Writing – review & editing, Validation, Supervision, Resources, Formal analysis.

Declaration of competing interest

The authors declare that they have no known competing financial interests or personal relationships that could have appeared to influence the work reported in this paper.

Acknowledgement

This research has been co-financed by the European Union and Greek national funds through the Operational Program Competitiveness, Entrepreneurship and Innovation, under the call RESEARCH – CREATE – INNOVATE (project code: T2EDK- 02504). In addition, part of this study has been researched during the PhD thesis of Dr. Marios Vasileiou. Furthermore, the authors would like to thank the editor and the anonymous reviewers for helpful and constructive feedback on an earlier version of this paper.

Appendix A

The two side parts, the left (P1) and the right (P2) are symmetrical to each other, and are joined with two central parts (P3) of the body on the upper

and lower side of the vehicle.

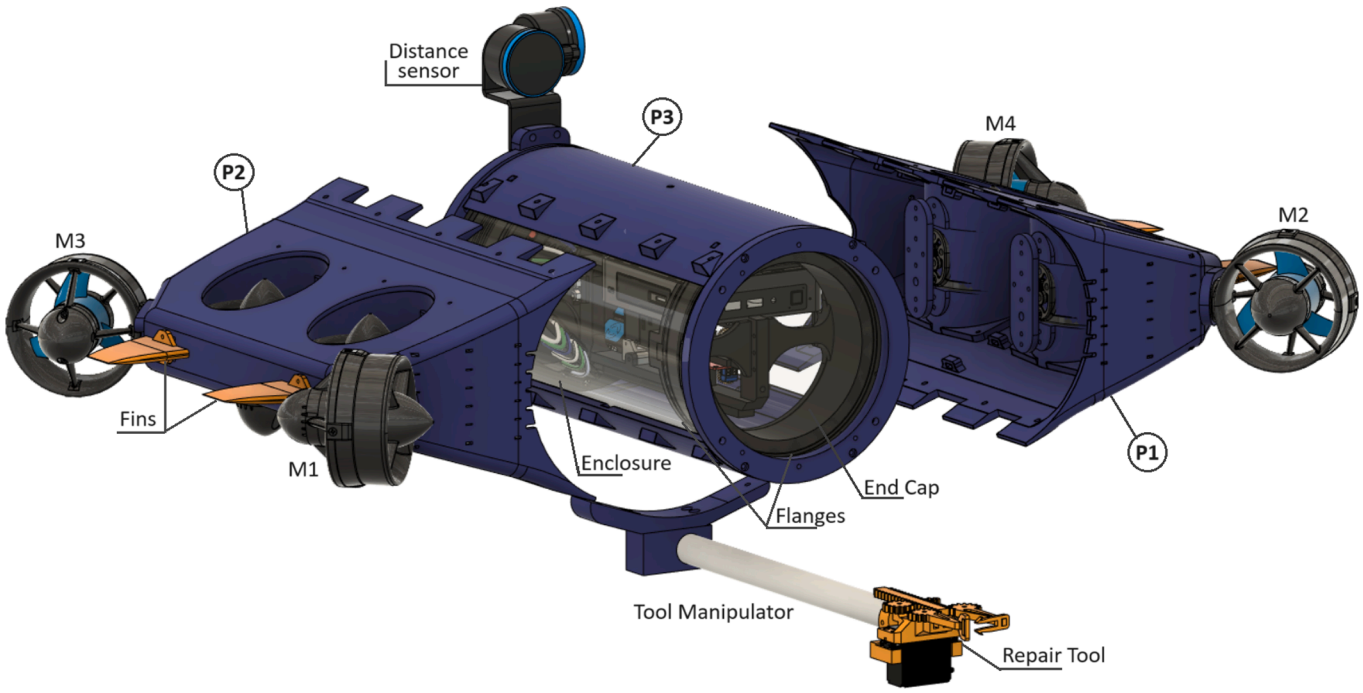

Fig. A1. Visualization of HROV main parts

Appendix B

Table B1
Results for each simulation.

	Surge		Sway		heave	
Velocity	Force	Drag Co.	Force	Drag Co.	Force	Drag Co.
0.2	1.18455	0.828542051	0.725745	0.507627581	6.35198	1.957857599
0.4	4.76823	0.833793226	2.91029	0.508905839	25.6038	1.97295152
0.6	10.8413	0.842558397	6.61902	0.514413482	57.9064	1.983152152
0.8	21.9632	0.960144928	11.5782	0.506153475	103.354	1.991036794
1	33.3985	0.93443288	17.723	0.495859213	162.188	1.999634812
1.2	46.9882	0.912950994	25.8799	0.502830082		
1.4	62.6532	0.894351697	35.649	0.50887654		
1.6	80.2753	0.877330285	46.8527	0.512054052		
1.8	100.074	0.864166444	59.6735	0.515297043		
2	121.967	0.853106989	74.0629	0.518038302		

Appendix C

((TITLE-ABS-KEY (underwater AND robotics) OR TITLE-ABS-KEY (underwater AND vehicle)) AND (TITLE-ABS-KEY (aquaculture) OR TITLE-ABS-KEY (mariculture) OR TITLE-ABS-KEY (fisheries))).

Appendix D. Supplementary multimedia data

Supplementary multimedia data to this article can be found online at:
1. Kalypso HROV | Autonomous navigation in aquaculture | Tetherless operation (Divers' view): https://youtu.be/X-kKrnqBOL0.
2. Kalypso HROV | Autonomous navigation trial in net cage | Tetherless operation (Internal Camera View): https://youtu.be/2wiFztigW6k.
3. Kalypso HROV | Net Tear Repair in Assisted Mode | Tethered operation (Divers' view): https://youtu.be/LeNBY0I28WY.
4. Kalypso HROV | Fish Mort Disposal in Assisted Mode | Tethered operation (surface view): https://youtube.com/shorts/q5p3irCtxFk.
5. Kalypso HROV | Object Removal in Assisted Mode | Tethered operation (Internal Camera view): https://youtu.be/WS3EVXUOBZo.

Data availability

The data that support the findings of this study are available from the corresponding author upon reasonable request.

References

Al-Hussaini, K., Zainol, S.M., Ahmed, R.B., Daud, S., 2018. IoT monitoring and automation data acquisition for recirculating aquaculture system using fog computing. *J. Comput. Hardware Eng.* 1.

Amory, A., Maehle, E., 2016. SEMBIO - a Small Energy-Efficient Swarm AUV. In Proceedings of the OCEANS 2016 MTS/IEEE Monterey; IEEE, September 2016; pp. 1–7.

Amundsen, H.B., Caharija, W., Pettersen, K.Y., 2021. Autonomous ROV inspections of aquaculture net pens using DVL. *IEEE J. Ocean. Eng.* 1–19. https://doi.org/10.1109/JOE.2021.3105285.

Arastehfar, S., Chew, C.-M., Jalalian, A., Gunawan, G., Yeo, K.S., 2019. A relationship between sweep angle of flapping pectoral fins and thrust generation. *J. Mech. Robot.* 11, doi:10.1115/1.4041697.

Barbieri, L., Bruno, F., Gallo, A., Muzzupappa, M., Russo, M.L., 2018. Design, prototyping and testing of a modular small-sized underwater robotic arm controlled through a master-slave approach. *Ocean Eng.* 158, 253–262. https://doi.org/10.1016/j.oceaneng.2018.04.032.

Berlinger, F., Dusek, J., Gauci, M., Nagpal, R., 2018. Robust maneuverability of a miniature, low-cost underwater robot using multiple fin actuation. *IEEE Robot Autom Lett* 3, 140–147. https://doi.org/10.1109/LRA.2017.2734969.

Berlinger, F., Duduta, M., Gloria, H., Clarke, D., Nagpal, R., Wood, R., 2018. A modular dielectric elastomer actuator to drive miniature autonomous underwater vehicles, In: Proceedings of the 2018 IEEE International Conference on Robotics and Automation (ICRA); IEEE, May 2018; pp. 3429–3435.

Bi, C.-W., Chen, Q.-P., Zhao, Y.-P., Su, H., Wang, X.-Y., 2020. Experimental investigation on the hydrodynamic performance of plane nets fouled by hydroids in waves. *Ocean Eng.* 213, 107839. https://doi.org/10.1016/j.oceaneng.2020.107839.

Biazi, V., Marques, C., 2023. Industry 4.0-based smart systems in aquaculture: a comprehensive review. *Aquac. Eng.* 103, 102360. https://doi.org/10.1016/j.aquaeng.2023.102360.

Blue Food Partnership; Friends of Ocean Action; World Economic Forum *Road to Sustainable Aquaculture Report*, 2022.

Brandt, M.A., Herland, S., Gutsch, M., Ludvigsen, H., Grøtli, E.I., 2023. Towards autonomous contact-free operations in aquaculture. *Ocean Eng.* 282, 115005. https://doi.org/10.1016/j.oceaneng.2023.115005.

Chicchon, M., Bedon, H., Del-Blanco, C.R., Sipiran, I., 2023. Semantic segmentation of fish and underwater environments using deep convolutional neural networks and learned active contours. *IEEE Access* 11, 33652–33665. https://doi.org/10.1109/ACCESS.2023.3262649.

D. Guihen, The Challenges and Opportunities for the Use of Robotic Autonomous Robotic Systems in Support of the Blue Economy, in: Proceedings of the Volume 10: Professor Ian Young Honouring Symposium on Global Ocean Wind and Wave Climate; Blue Economy Symposium; Small Maritime Nations Symposium; American Society of Mechanical Engineers, June 11 2023.

DeVries, L., Kutzer, M.D.M., Bass, A., Richmond, R., 2020. Hull shape actuation for speed regulation in an underwater vehicle. *J. Mech. Robot.* 12, doi:10.1115/1.4045038.

Duecker, D.A., Bauschmann, N., Hansen, T., Kreuzer, E., Seifried, R., 2020. HippoCampusX – A Hydrobatic Open-Source Micro AUV for Confined Environments. In: Proceedings of the 2020 IEEE/OES Autonomous Underwater Vehicles Symposium (AUV)(50043); IEEE, September 30 2020; pp. 1–6.

FAO, The State of World Fisheries and Aquaculture 2020, Sustainability in Action; Rome, 2020.

FAO The State of World Fisheries and Aquaculture 2022. Towards Blue Transformation; Rome, 2022.

Ferreira, C.Z., Cardoso, R., Meza, M.E.M., Ávila, J.P.J., 2018. Controlling tracking trajectory of a robotic vehicle for inspection of underwater structures. *Ocean Eng.* 149, 373–382. https://doi.org/10.1016/j.oceaneng.2017.12.032.

Fossen, T.I., 2011. Handbook of Marine Craft Hydrodynamics and Motion Control; Wiley, 2011; ISBN 9781119991496.

Fu, J., Liu, D., He, Y., Cheng, F., 2024. Autonomous net inspection and cleaning in sea-based fish farms: a review. *Comput. Electron. Agric.* 227, 109609. https://doi.org/10.1016/j.compag.2024.109609.

García-Valdovinos, L.G., Salgado-Jiménez, T., Bandala-Sánchez, M., Nava-Balanzar, L., Hernández-Alvarado, R., Cruz-Ledesma, J.A., 2014. Modelling, design and robust control of a remotely operated underwater vehicle. *Int. J. Adv. Rob. Syst.* 11, 1. https://doi.org/10.5772/56810.

Gotts, C., Hall, B., Beaumont, O., Chen, Z., Cleaver, W., England, J., White, D., Thornton, B., 2022. Development of a prototype autonomous inspection robot for offshore riser cables. *Ocean Eng.* 257, 111485. https://doi.org/10.1016/j.oceaneng.2022.111485.

Guillen, J., Motova, A., 2013. Summary of the 2013 Economic Performance Report on the EU Aquaculture Sector (STECF 13-30); Brussels, Belgium, 2013.

Hackbarth, A., Kreuzer, E., Solowjow, E., 2015. HippoCampus: A Micro Underwater Vehicle for Swarm Applications, in: Proceedings of the 2015 IEEE/RSJ International Conference on Intelligent Robots and Systems (IROS); IEEE, September 2015; pp. 2258–2263.

Hammoud, A., Sahili, J., Madi, M., Maalouf, E., 2021. Design and dynamic modeling of ROVs: estimating the damping and added mass parameters. *Ocean Eng.* 239, 109818. https://doi.org/10.1016/j.oceaneng.2021.109818.

Ji, Y., Wei, Y., Liu, J., An, D., 2023. Design and realization of a novel hybrid-drive robotic fish for aquaculture water quality monitoring. *J. Bionic Eng.* 20, 543–557. https://doi.org/10.1007/s42235-022-00282-1.

Johansson, D., Juell, J.-E., Oppedal, F., Stiansen, J.-E., Ruohonen, K., 2007. The influence of the pycnocline and cage resistance on current flow, oxygen flux and swimming behaviour of atlantic salmon (*Salmo Salar* L.) in production cages. *Aquaculture* 265, 271–287. https://doi.org/10.1016/j.aquaculture.2006.12.047.

Kadiyam, J., Parashar, A., Mohan, S., Deshmukh, D., 2020. Actuator fault-tolerant control study of an underwater robot with four rotatable thrusters. *Ocean Eng.* 197, 106929. https://doi.org/10.1016/j.oceaneng.2020.106929.

Kitowski, Z., Soliński, R., 2016. Application of domestic unmanned surface vessels in the area of internal security and maritime economy — capacities and directions for development. Scientific J. Polish Naval Acad. 206, 67–83. https://doi.org/10.5604/0860889x.1224747.

Kruusmaa, M., Gkliva, R., Tuhtan, J.A., Tuvikene, A., Alfredsen, J.A., 2020. Salmon behavioural response to robots in an aquaculture sea cage. *R. Soc. Open Sci.* 7, 191220. https://doi.org/10.1098/rsos.191220.

Kyrgiakos, L.S., Kleftodimos, G., Vlontzos, G., Pardalos, P.M., 2023. A systematic literature review of data envelopment analysis implementation in agriculture under the prism of sustainability. *Oper. Res.* 23, 7. https://doi.org/10.1007/s12351-023-00741-5.

Lamraoui, H.C., Qidan, Z., Bouzid, Y., 2022. Improved active disturbance rejecter control for trajectory tracking of unmanned surface vessel. *Mar. Syst. Ocean Technol.* 17, 18–26. https://doi.org/10.1007/s40868-021-00110-x.

Lemos, R.L., Marques, C.H., El Halal, Y.B., dos Santos, E.D., 2021. Two novel marine thruster concepts based on the Coanda effect. *Mar. Syst. Ocean Technol.* 16, 14–22. https://doi.org/10.1007/s40868-021-00092-w.

Li, J.H., Kim, J.T., Lee, M.J., Lee, W.S., Kang, H.J., Han, S.C., Lee, J.W., Kwak, H.W., 2014. Conceptual design of optimal thrust system for efficient cable burying of ROV threncher. In: Proceedings of the 2014 Oceans - St. John's; IEEE, September 2014; pp. 1–5.

Li, M., Yu, C., Zhang, X., Liu, C., Lian, L., 2023. Fuzzy adaptive trajectory tracking control of work-class ROVs considering thruster dynamics. *Ocean Eng.* 267, 113232. https://doi.org/10.1016/j.oceaneng.2022.113232.

Lin, T.X., Tao, Q., Zhang, F., 2020. Planning for Fish Net Inspection with an Autonomous OSV, in: Proceedings of the 2020 International Conference on System Science and Engineering (ICSSE); IEEE, August 2020; pp. 1–5.

Liu, Y., Design, B.-T., 2020. Analysis, and integration of a new two-degree-of-freedom articulated multi-link robotic tail mechanism. *J. Mech. Robot.* 12, doi:10.1115/1.4045842.

Liu, C., Wang, Z., Li, Y., Zhang, Z., Li, J., Xu, C., Du, R., Li, D., Duan, Q., 2023. Research progress of computer vision technology in abnormal fish detection. *Aquac. Eng.* 103, 102350. https://doi.org/10.1016/j.aquaeng.2023.102350.

Mandal, A., Ghosh, A.R., 2023. Role of artificial intelligence (AI) in fish growth and health status monitoring: a review on sustainable aquaculture. *Aquac. Int.* https://doi.org/10.1007/s10499-023-01297-z.

Mansour, A., Liu, D., Paulling, J.R., 2008. The Principles of Naval Architecture Series; Jersey City, NJ, 2008.

Marras, S., Porfiri, M., 2012. Fish and robots swimming together: attraction towards the robot demands biomimetic locomotion. *J. R. Soc. Interface* 9, 1856–1868. https://doi.org/10.1098/rsif.2012.0084.

Meyer, B., Ehlers, K., Isokeit, C., Maehle, E., 2017. The Development of the Modular Hard-and Software Architecture of the Autonomous Underwater Vehicle MONSUN, in: Proceedings of the ISR/Robotik 2014; 41st International Symposium on Robotics; June 2017; pp. 1–6.

Muzammal, H., Mehdi, S.A., Ahmed Hanif, M., Maurelli, F., 2021. Design and Fabrication of a Low-Cost 6 DoF Underwater Vehicle. In Proceedings of the 2021 European Conference on Mobile Robots (ECMR); IEEE, August 2021; pp. 1–5.

Ohrem, S.J., Kelasidi, E., Bloecher, N., 2020. Analysis of a Novel Autonomous Underwater Robot for Biofouling Prevention and Inspection in Fish Farms. In: Proceedings of the 2020 28th Mediterranean Conference on Control and Automation (MED); IEEE, September 2020; pp. 1002–1008.

Osen, O., Sandvik, R.-I., Trygstad, J.-B., Rogne, V., Zhang, H., 2017. A novel low cost ROV for Aquaculture application, in: Proceedings of the OCEANS 2017 - Anchorage; 2017; pp. 1–7.

Osen, O.L., Leinan, P.M., Blom, M., Bakken, C., Heggen, M., Zhang, H., 2018. A novel sea farm inspection platform for norwegian aquaculture application, in: Proceedings of the OCEANS 2018 MTS/IEEE Charleston; IEEE, October 2018, pp. 1–8.

Osterloh, C., Pionteck, T., Maehle, E., 2012. MONSUN II: A Small and Inexpensive AUV for Underwater Swarms. In Proceedings of the ROBOTIK 2012; 7th German Conference on Robotics; May 2012; pp. 1–6.

PX4 Autopilot PX4-ECL GitHub Library Available online: https://github.com/PX4/PX4-ECL (accessed on 5 December 2024).

Qiao, X., Bao, J., Zeng, L., Zou, J., Li, D., 2017. An automatic active contour method for sea cucumber segmentation in natural underwater environments. *Comput. Electron. Agric.* 135, 134–142. https://doi.org/10.1016/j.compag.2017.02.008.

Ridolfi, A., Costanzi, R., Fanelli, F., Monni, N., Allotta, B., Bianchi, S., Conti, R., Gelli, J., Gori, L., Pugi, L., et al., 2016. FeelHippo: a low-cost autonomous underwater vehicle for subsea monitoring and inspection, in: Proceedings of the 2016 IEEE 16th International Conference on Environment and Electrical Engineering (EEEIC); IEEE, June 2016; pp. 1–6.

Rigatos, G., Siano, P., Zouari, F., Ademi, S., 2020. Nonlinear optimal control of autonomous submarines' diving. *Mar. Syst. Ocean Technol.* 15, 57–69. https://doi.org/10.1007/s40868-019-00070-3.

Rigby, B., Davis, R., Bavington, D., Baird, C., 2017. Industrial aquaculture and the politics of resignation. *Mar. Policy* 80, 19–27. https://doi.org/10.1016/j.marpol.2016.10.016.

Rowan, N.J., 2023. The role of digital technologies in supporting and improving fishery and aquaculture across the supply Chain – Quo Vadis? *Aquac Fish* 8, 365–374. https://doi.org/10.1016/j.aaf.2022.06.003.

Rymansaib, Z., Thomas, B., Treloar, A.A., Metcalfe, B., Wilson, P., Hunter, A., 2023. A Prototype autonomous robot for underwater crime scene investigation and emergency response. *J Field Robot* 40, 983–1002. https://doi.org/10.1002/rob.22164.

Santos-Ballardo, D.U., Rossi, S., Hernández, V., Gómez, R.V., del Carmen Rendón-Unceta, M., Caro-Corrales, J., Valdez-Ortiz, A., 2015. A simple spectrophotometric method for biomass measurement of important microalgae species in aquaculture. *Aquaculture* 448, 87–92. https://doi.org/10.1016/j.aquaculture.2015.05.044.

Shakouri, M., 2003. Impact of cage culture on sediment chemistry. A case study in mjoifjordur. Fisheries Training Programme, The United Nations University 2003.

Simbeye, D.S., Yang, S.F., 2014. Water quality monitoring and control for aquaculture based on wireless sensor networks. *J. Networks* 9, doi:10.4304/jnw.9.4.840-849.

Sitler, J.L., Wang, L., 2022. A modular open-source continuum manipulator for underwater remotely operated vehicles. *J. Mech. Robot.* 14, doi:10.1115/1.4054309.

Skaldebø, M., Ohrem, S.J., Amundsen, H.B., Kelasidi, E., Bloecher, N., 2023. Framework for autonomous navigation for a permanent resident aquaculture net grooming robot, in: Proceedings of the 2023 31st Mediterranean Conference on Control and Automation (MED), IEEE, June 26 2023, pp. 356–363.

Sønstabø, H.J., 2017. ROV Tool to Repair Fish Cages, Norwegian University of Life Sciences, 2017.

Stien, L.H., Nilsson, J., Hevrøy, E.M., Oppedal, F., Kristiansen, T.S., Lien, A.M., Folkedal, O., 2012. Skirt around a salmon sea cage to reduce infestation of salmon lice resulted in low oxygen levels. *Aquac. Eng.* 51, 21–25. https://doi.org/10.1016/j.aquaeng.2012.06.002.

Sumaila, U.R., Pierruci, A., Oyinlola, M.A., Cannas, R., Froese, R., Glaser, S., Jacquet, J., Kaiser, B.A., Issifu, I., Micheli, F., et al., 2022. Aquaculture over-optimism? *Front. Mar. Sci.* 9, 10.3389/fmars.2022.984354.

Sung, W.-T., Chen, J.-H., Wang, H.-C., 2014. Remote Fish Aquaculture Monitoring System Based on Wireless Transmission Technology. In: Proceedings of the 2014 International Conference on Information Science, Electronics and Electrical Engineering; IEEE, April 2014; pp. 540–544.

Tang, S., Xue, N., Liu, K., Wang, D., Ye, J., Fan, T., 2023. Motion control for an open-frame work-class ROV in current using an adaptive super-twisting disturbance observer. *Ocean Eng.* 280, 114723. https://doi.org/10.1016/j.oceaneng.2023.114723.

Tiwari, K., Krishnankutty, P., 2021. Dynamic positioning of an oceanographic research vessel using fuzzy logic controller in different sea states. *Mar. Syst. Ocean Technol.* 16, 221–236. https://doi.org/10.1007/s40868-021-00105-8.

Vasileiou, M., Manos, N., Kavallieratou, E., 2023. MURA: a multipurpose underwater robotic arm mounted on kalypso UUV in aquaculture. *Mar. Syst. Ocean Technol.* https://doi.org/10.1007/s40868-023-00129-2.

Vasileiou, M., Manos, N., Vasilopoulos, N., Douma, A., Kavallieratou, E., 2024. Kalypso autonomous underwater vehicle: a 3D-printed underwater vehicle for inspection at fisheries. *J. Mech. Robot.* 16, doi:10.1115/1.4062355.

Von Borstel Luna, F.D., de la Rosa Aguilar, E., Suarez Naranjo, J., Gutierrez Jaguey, J., 2017. Robotic system for automation of water quality monitoring and feeding in aquaculture shadehouse. *IEEE Trans Syst Man Cybern Syst* 47, 1575–1589. https://doi.org/10.1109/TSMC.2016.2635649.

SNAME, 1950. The Society of Naval Architects and Marine Engineers Nomenclature for Treating the Motion of a Submerged Body through a Fluid. *Technical and Research Bulletin* **1950**.

Waltman, L., Ecken, N., 2010. VOSViewer: Visualizing Scientifc Landscapes. https://www.vosviewer.com/.

Wang, Y., Yu, X., An, D., Wei, Y., 2021. Underwater image enhancement and marine snow removal for fishery based on integrated dual-channel neural network. *Comput. Electron. Agric.* 186, 106182. https://doi.org/10.1016/j.compag.2021.106182.

Wu, C.-J., 2018. 6-DoF Modelling and Control of a Remotely Operated Vehicle. Flinders University.

Wu, Y., Duan, Y., Wei, Y., An, D., Liu, J., 2022. Application of Intelligent and unmanned equipment in aquaculture: a review. *Comput. Electron. Agric.* 199, 107201. https://doi.org/10.1016/j.compag.2022.107201.

Xie, B., Jin, Y., Faheem, M., Gao, W., Liu, J., Jiang, H., Cai, L., Li, Y., 2023. Research progress of autonomous navigation technology for multi-agricultural scenes. *Comput. Electron. Agric.* 211, 107963. https://doi.org/10.1016/j.compag.2023.107963.

Yu, S.-C., Yuh, J., Kim, J., 2013. Armless underwater manipulation using a small deployable agent vehicle connected by a smart cable. *Ocean Eng.* 70, 149–159. https://doi.org/10.1016/j.oceaneng.2013.06.006.

Yu, F., Zhu, Q., Chen, Y., 2023. Adaptive fractional-order fast-terminal-type sliding mode control for underwater vehicle-manipulator systems. *J. Mech. Robot.* 15, doi:10.1115/1.4056378.

Yue, K., Shen, Y., 2022. An overview of disruptive technologies for aquaculture. *Aquac Fish* 7, 111–120. https://doi.org/10.1016/j.aaf.2021.04.009.

Zhao, C., Thies, P.R., Johanning, L., 2022. Offshore inspection mission modelling for an ASV/ROV system. *Ocean Eng.* 259, 111899. https://doi.org/10.1016/j.oceaneng.2022.111899.

Zheng, T., Branson, D.T., Guglielmino, E., Kang, R., Medrano Cerda, G.A., Cianchetti, M., Follador, M., Godage, I.S., Caldwell, D.G., 2013. Model validation of an octopus inspired continuum robotic arm for use in underwater environments. *J. Mech. Robot.* 5, doi:10.1115/1.4023636.